Isogeochemical Characterization of Mountain System Recharge Processes in the Sierra Nevada, California

Sandra Armengol[1], Hoori Ajami[1], James O'sickman[1], and Lucia Ortega[2]

[1]University of California
[2]International Atomic Energy Agency (IAEA)

December 8, 2022

Abstract

Mountain System Recharge (MRS) processes are the natural recharge pathways in arid and semi-arid mountainous regions. However, MSR processes are often poorly understood and characterized in hydrologic models. Mountains are the primary source of water supply to valley aquifers via multiple pathways including lateral groundwater flow from the mountain block (Mountain-block Recharge, MBR) and focused recharge from mountain streams contributing to mountain front recharge (MFR) at the piedmont zone. Here, we present a multi-tool isogeochemical approach to characterize mountain flow paths and MSR processes in the northern Tulare basin, California. We used groundwater chemistry data to delineate hydrochemical facies and explain the chemical evolution of groundwater from the Sierra Nevada to the Central Valley aquifer. Isotope tracers helped to validate MSR processes. Novel application of End-Member Mixing Analysis (EMMA) using conservative chemical components revealed three MSR end-members: (1) evaporated Ca-HCO3 water type associated with MFR, (2) non-evaporated Ca-HCO3 and Na-HCO3 water types with short residence times associated with shallow MBR, and (3) Na-HCO3 groundwater type with long residence time associated with deep MBR. We quantified the contribution of each MSR process to the valley aquifer using mixing ratio calculation (MIX). Our results show that deep MBR is a significant component of recharge representing more than 50% of the valley groundwater. Greater hydraulic connectivity between the Sierra Nevada and Central Valley has significant implications for parameterizing Central Valley groundwater flow models and improving groundwater management. Our framework is useful for understanding MSR processes in other snow-dominated mountain watersheds.

1

1 **Isogeochemical Characterization of Mountain System Recharge Processes in the Sierra**
2 **Nevada, California**

3 Sandra Armengol[1]†, Hoori Ajami[1], James O'Sickman[1], Lucia Ortega[2]

4 [1] Department of Environmental Sciences, University of California, Riverside, CA, USA.

5 [2] International Atomic Energy Agency (IAEA), Vienna, Austria.

6 Corresponding author: Sandra Armengol (sarmengo@ucr.edu)

7 †Department of Environmental Sciences, University of California, Riverside, Room 2319
8 Geology, Riverside, California 92521.

9 **Key Points:**

10 **A multi-tool isogeochemical approach differentiates among mountain recharge pathways.**

11 **Incorporating chemical reactions in the End-Member Mixing Analysis strongly improves**
12 **mixing ratio calculation.**

13 **Mountain block recharge originating from the Sierra Nevada accounts on average for more**
14 **than 50% of recharge in the southern Central Valley.**

15

16 **Keywords: Mountain System Recharge, Hydrogeochemisty, End-Member Mixing Analysis,**
17 **Mountain Front Recharge, Mountain Block Recharge**

18

19

20

21

22 `

23

24

25

26

27

28 **Abstract**

29 Mountain System Recharge (MRS) processes are the natural recharge pathways in arid and semi-
30 arid mountainous regions. However, MSR processes are often poorly understood and
31 characterized in hydrologic models. Mountains are the primary source of water supply to valley
32 aquifers via multiple pathways including lateral groundwater flow from the mountain block
33 (Mountain-block Recharge, MBR) and focused recharge from mountain streams contributing to
34 mountain front recharge (MFR) at the piedmont zone. Here, we present a multi-tool
35 isogeochemical approach to characterize mountain flow paths and MSR processes in the northern
36 Tulare basin, California. We used groundwater chemistry data to delineate hydrochemical facies
37 and explain the chemical evolution of groundwater from the Sierra Nevada to the Central Valley
38 aquifer. Isotope tracers helped to validate MSR processes. Novel application of End-Member
39 Mixing Analysis (EMMA) using conservative chemical components revealed three MSR end-
40 members: (1) evaporated $Ca-HCO_3$ water type associated with MFR, (2) non-evaporated Ca-
41 HCO_3 and $Na-HCO_3$ water types with short residence times associated with shallow MBR, and
42 (3) $Na-HCO_3$ groundwater type with long residence time associated with deep MBR. We
43 quantified the contribution of each MSR process to the valley aquifer using mixing ratio
44 calculation (MIX). Our results show that deep MBR is a significant component of recharge
45 representing more than 50% of the valley groundwater. Greater hydraulic connectivity between
46 the Sierra Nevada and Central Valley has significant implications for parameterizing Central
47 Valley groundwater flow models and improving groundwater management. Our framework is
48 useful for understanding MSR processes in other snow-dominated mountain watersheds.

49 **1. Introduction**

50 Seasonal snowpacks and glaciers supply water to more than 16% of the global population
51 (Barnett, 2005), and 24% of lowland populations rely on runoff from mountainous watersheds
52 (Viviroli et al., 2020). While the contribution of mountain watersheds to streamflow is well
53 known (Viviroli et al., 2020), the mechanisms of groundwater recharge processes in high-
54 elevation mountain ranges are poorly understood (Gleeson and Manning, 2008). Likewise, the
55 degree of hydraulic connectivity between the mountains and valley-fill aquifers is still uncertain
56 (de Vries and Simmers, 2002). Prolonged droughts and reduced snowpack in the western US
57 have increased reliance on groundwater (Scanlon et al., 2005), causing overexploitation of major
58 aquifers, e.g., California's Central Valley aquifer. Projected increases in the frequency and
59 intensity of droughts, warmer temperatures (Seager et al., 2007; Diffenbaugh et al., 2015), and
60 snow to rain transition (Berghuijs et al., 2014) are expected to alter the magnitude and direction
61 of recharge rates. However, our ability to accurately estimate recharge in mountain catchments is
62 limited due to the complexity of recharge processes and lack of direct recharge observations
63 (Ajami et al., 2011; Bales et al., 2006).

64

65 Various terminologies have been used to describe recharge processes in a mountain-valley
66 aquifer system (Markovich et al., 2019). Conceptually, a mountain-valley aquifer system consists
67 of two units: a mountain aquifer unit extending from headwaters to the piedmont zone where
68 mountains intersect alluvial deposits (Welch and Allen, 2012), and a valley bottom aquifer unit
69 with boundaries starting at the piedmont zone. We define five recharge pathways along the
70 mountain-valley aquifer continuum (Figure 1). The two main recharge pathways recharging the
71 mountain aquifer are diffuse and focused Mountain Aquifer Recharge (MAR). Diffuse MAR
72 results from snowmelt and rainfall infiltration into the mountain block and focused MAR is from

73 streamflow infiltration and seepage from lakes in the mountain block. The three main pathways
74 recharging the valley aquifer are: Diffuse valley aquifer recharge (VAR), due to rainfall and
75 irrigation infiltration in the valley floor; focused mountain front recharge (MFR), because of
76 streamflow infiltration in the piedmont zone; and mountain block recharge (MBR) as a result of
77 lateral subsurface flow from the mountain aquifer unit to the adjacent valley aquifer. MFR and
78 MBR may consist of different flow paths with distinct geochemical signatures and residence
79 time. These pathways are collectively called mountain system recharge (MSR).
80
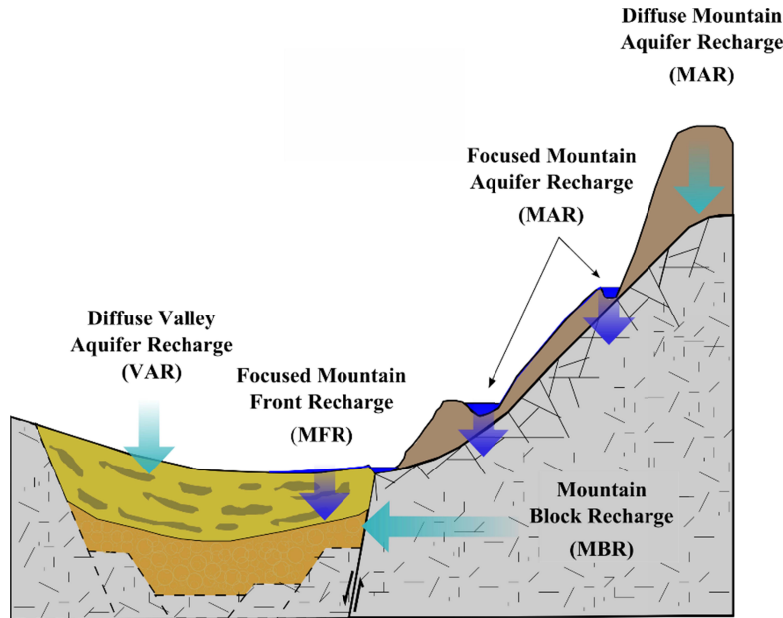
Figure 1. Conceptual illustration of five different recharge pathways in a mountain-valley aquifer system.

84 MBR and MFR constitute significant recharge components in many arid and semi-arid aquifers
85 (Wilson and Guan, 2004). VAR in arid and semi-arid aquifers is very small due to small
86 precipitation and high evapotranspiration rates. Given differences in infiltration location and
87 residence times of MSR pathways, it is essential to distinguish MSR pathways as they may
88 respond differently to changes in hydroclimate and vegetation conditions (Markovich et al.,
89 2019). While some hydrologists assumed that bedrock is impermeable, the application of
90 geochemical tracers combined with heat and flow modeling demonstrated that MBR contributes
91 5% to 50% of total recharge (Markovich et al., 2019; Meixner et al., 2016; Aishlin &
92 McNamara, 2011; Manning and Solomon, 2003). A recent synthesis of recharge from mountain
93 aquifers showed that 61 – 93% of MAR discharges via streams (Meixner et al., 2016) and
94 eventually contributes to MFR (Abdulghaffar & Wood, 1996; Coes and Pool, 2007; Goodrich et
95 al., 200; Schreiner-McGraw et al., 2019).
96 Various methods have been implemented to estimate MSR ranging from empirical relationships
97 (e.g., Maxey-Eakin (1949)) to spatially distributed water balance models such as the Basin
98 Characterization Model (Flint et al., 2004). Accurate MSR quantification requires characterizing
99 the mountain aquifer unit and groundwater circulation depth (Frisbee et al., 2017), as well as the
100 flow paths from the mountain block to the adjacent aquifers. Water balance models require a
101 large amount of data typically unavailable in mountainous catchments due to extreme weather
102 especially during winter, limited access due to complex terrain, and the presence of few

103 mountain wells. Alternately, the chloride mass balance method (CMB) has been extensively used
104 to estimate recharge rates in mountain catchments (Aishlin & McNamara, 2011). Chloride is
105 considered a conservative solute as it is rarely present in the mountain bedrock and is neither
106 evaporated nor transpired. Bazuhair & Wood (1996) used the CMB method to estimate MBR
107 from the western Saudi Arabia mountains to arid alluvial aquifers. Annual MBR was 3 to 4% of
108 mean annual precipitation with 30 to 50% error in the short-term dataset. In the Dry Creek
109 watershed in Idaho, CMB results showed that 14% of precipitation and 44% of headwater areas
110 contribute to MBR (Aishlin and McNamara, 2011). Annual MBR estimates from the Yucca
111 Mountain in Nevada and Black Mesa in Arizona were 3 to 15 % and 3 to 7% of mean annual
112 precipitation, respectively (Zhu et al., 2003). Application of the CMB method in recharge
113 studies is challenging as chloride retention in soils is not well understood (Shaw et al., 2014),
114 and in low electrical conductivity environments such as snow-dominated mountain systems,
115 chloride is not entirely conservative (Shaw et al., 2014). Furthermore, the CMB method only
116 accounts for a single tracer and more than one tracer is usually needed to describe mixing
117 dynamics in complex mountain-valley systems.
118
119 Christopherson and Hooper (1992) and Hooper et al. (1990) combined multiple tracers using a
120 multivariate statistical analysis method, (EMMA), to identify water sources in streamflow. The
121 application of EMMA has been instrumental in identifying MSR sources (e.g., Wahi et al., 2008)
122 and its partitioning. Wahi and others (2008) applied a mixing model using oxygen and hydrogen
123 isotopes in the Upper San Pedro River Basin, Arizona, attributing 70% of the MSR, to winter
124 and 30% to summer precipitation. Peng et al. (2018) applied EMMA to oxygen and hydrogen
125 groundwater isotopes and electrical conductivity (EC) data from three alluvial fans in eastern
126 Taiwan. They attributed 70 % of the MSR to MFR and MBR, and the remainder to VAR. They
127 showed MBR is mainly controlled by the degree of mountain bedrock fracturing, while MFR is
128 impacted by streambed permeability and slope. Liu and Yamanaka (2012) applied EMMA to
129 oxygen and hydrogen groundwater isotopes and major dissolved solutes, and identified distance
130 from the river and topography as important factors controlling MFR. Frisbee et al. (2011) applied
131 EMMA to EC, calcium, magnesium, potassium, silica, and $\delta^{18}O$ and δ^2H of groundwater in two
132 mountain watersheds in the Southwestern United States. They determined a deep circulation
133 flow depth of 1 to 1.5 km depth, controlling stream chemistry and flow dynamics across the
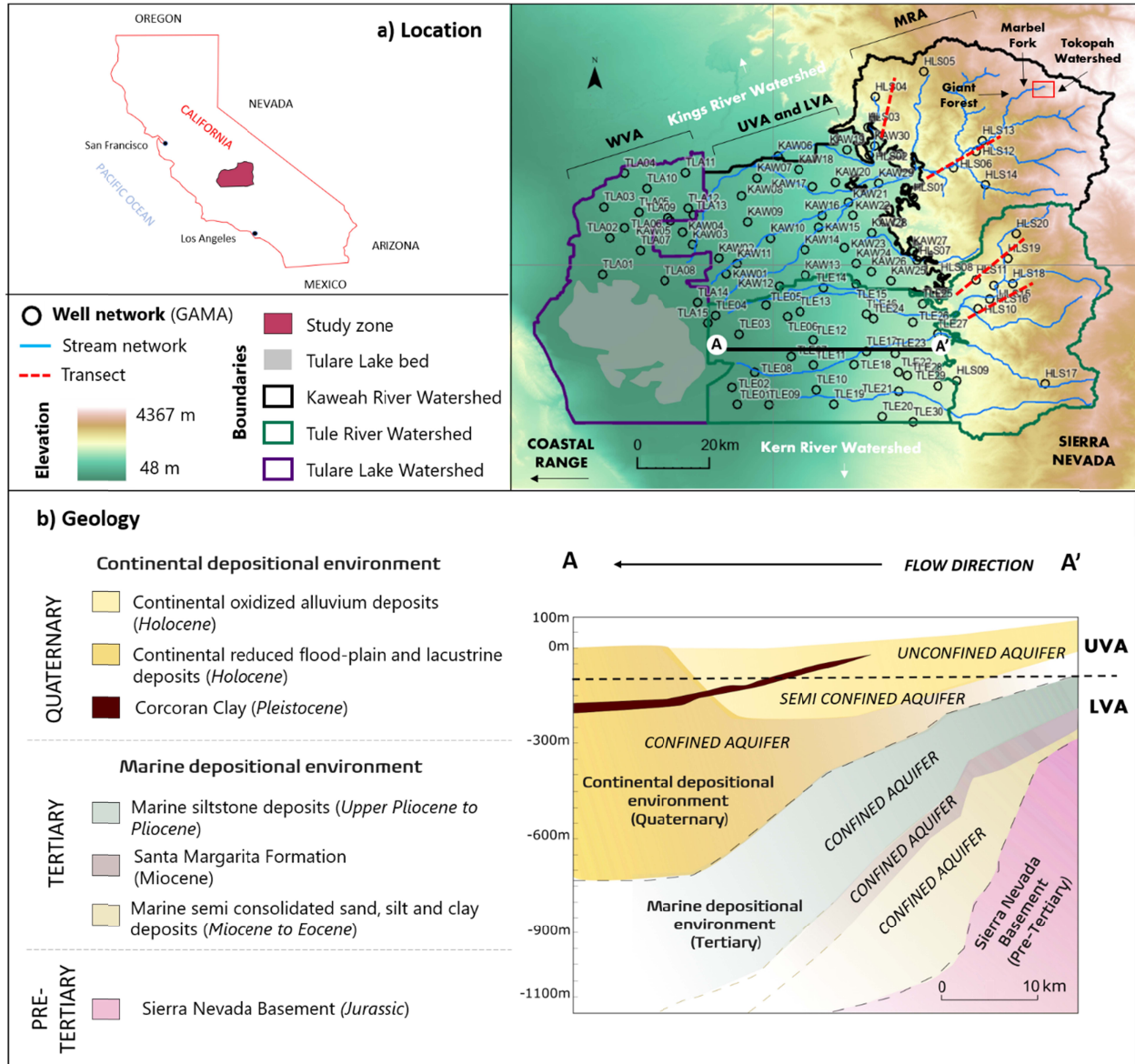134 watershed.
135
136 Although EMMA has been successfully implemented in many studies, its application depends on
137 selecting conservative tracers (Christophersen and Hooper, 1992; Hooper, 2003; Carrera et al.,
138 2004; Barthold et al., 2011). Choosing conservative tracers is often challenging, mainly due to
139 water-rock reactions and anthropogenic pollution affecting groundwater chemistry (Parkhurst,
140 1997; Carrera et al., 2004). The non-conservative behavior of species significantly decreases
141 dataset size, reducing the representativeness of the groundwater system (Rueedi et al., 2015). To
142 broaden the application of EMMA using non-conservative tracers, Pelizardi et al. (2017)
143 combined non-conservative solutes to create conservative chemical components. The
144 conservative components are created by defining the chemical system in a stoichiometric matrix,
145 *S*. The *S* matrix contains the reactions, the species, and the stoichiometric coefficients. MIX
146 estimates mixing ratios by using conservative species concentration while acknowledging
147 uncertainty in end-member concentrations using a maximum likelihood method.
148

149 In the California Central Valley aquifer system, more than 75% of agricultural water supply
150 derives from precipitation in the Sierra Nevada (Rosenthal and Dozier, 1996), and MSR from the
151 Sierra Nevada constitutes a significant recharge component, 20% compared to 11% from diffuse
152 recharge (Meixner et al., 2016). However, significant uncertainties exist in the Sierra Nevada's
153 MSR estimates, and no information about groundwater flow paths from headwaters to the
154 Central Valley aquifer system is available. Our objective is to address this critical knowledge gap
155 by using multiple tracers and EMMA to characterize groundwater flow paths from the southern
156 Sierra Nevada mountain aquifers to the northern Tulare basin in California's Central Valley and
157 differentiate MFR, MBR, and VAR processes. The Tulare basin is one of the most over-drafted
158 basins in California. Groundwater storage decreased by about 3 km^3/yr over the last decades
159 (Alam et al., 2019), and the depletion rate was three times higher during the 2006-2010 and
160 2012-2016 droughts (Scanlon et al., 2012; Xiao et al., 2017). We used hydrochemical and
161 isotope data from the US Geological Survey Groundwater Ambient Monitoring and Assessment
162 (GAMA) program (Bennett et al., 2017) and implemented a multi-tool isogeochemical approach
163 combined with EMMA and MIX analysis to answer three main research questions: 1) How does
164 groundwater chemistry vary in the mountain-valley aquifer system of the northern Tulare basin?
165 2) How to differentiate MAR, MFR, and MBR processes using major chemical solutes and
166 isotope tracers?, and 3) What is the hydraulic connectivity between the mountain and valley
167 groundwater systems?
168
2. Materials and Methods

2.1. Study Area

171 The study area constitutes the northern Tulare Basin in California, with an area of 9,914 km2
172 extending between the Coastal Range in the west and the Sierra Nevada in the east. The area
173 encompasses the Kaweah River, Tule River, and Tulare Lake watersheds (Figure 2a).
174 Historically, the Tule River, Kaweah River, and the Kings River were discharging into the
175 currently dry Tulare Lake. Elevation varies from 4421 masl on Mount Whitney to below sea
176 level in the valley significantly impacting the climate. Lowlands (< 1,500 m elevation) and mid-
177 elevation montane regions (1,500 – 2,500 m) have Mediterranean to semi-arid desert climate
178 with hot and dry summers and cold winters (Boiano et al., 2005). Regions above 2,500 m
179 elevation have Alpine climate with mean temperature lower than 10oC (Boiano et al., 2005).
180 Mean annual precipitation varies between 150 mm in Lowlands to over 1000 mm at elevations
181 above 2500 m, and mainly occurs from November to March (Faunt et al., 2016; NOAA, 2022).

Figure 2. a) Location of the study area comprising the Kaweah River, Tule River, and Tulare Lake watersheds, GAMA network, and four regions defined in this study: Mountain Range Aquifer (MRA), Upper Valley Aquifer (UVA), Lower Valley Aquifer (LVA) and Western Valley Aquifer (WVA). b) Modified geologic cross section (A-A') from Lofgren and Klausing (1969) with the main hydrogeological units. Vertical exaggeration is x26.

2.2. Geology and Hydrogeology

The study region physiography consists of the Sierra Nevada in the east and the Central Valley. The Sierra Nevada comprises Jurassic granitic rocks, including granodiorite containing quartz, potassium feldspar, plagioclase feldspar, biotite, and hornblende (Huber, 1987). The Central Valley sedimentary basin mainly consists of Tertiary marine to Quaternary continental sediments deposited over a crystalline pre-tertiary basement. On the west, the study region is bounded by faulted sedimentary, volcanic, and metamorphic rocks of the Coastal Range (Lofren and Klausing, 1969) (Figure 2b). Six central Tertiary to Quaternary sedimentary units are identified

195 from bottom to top in the valley: (1) Marine semi-consolidated deposits (Tertiary), (2) the Santa
196 Margarita Formation (Tertiary), (3) Marine siltstone deposits (Tertiary), (4) Lacustrine and
197 flood-plain deposits (Quaternary), (5) Oxidized continental deposits (Quaternary), and (6) the
198 Corcoran clay (Quaternary) (Figure 2b).

199 • The Marine semi-consolidated deposits with thicknesses between 60 m to 460 m are
200 Miocene to Eocene age marine sand, silt, and clay sequence (Park and Weddle, 1959;
201 Hilton et al., 1963). These layers behave as a confined aquifer and contain highly saline
202 water (Lofren and Klausing, 1969).
203 • The Santa Margarita Formation (Diepenbrock, 1933) is a Miocene age marine unit with
204 50 m to 160 m thickness and mainly composed of fine gravel, fine to coarse sand, very
205 fine green to gray clay, and shale facies (Hoots et al., 1954). This unit is the deepest
206 freshwater aquifer in the study area used for agriculture (Lofren and Klausing, 1969).
207 • The marine siltstone Pliocene and Pliocene deposits with 190 m to 800 m thickness are
208 siltstone diatomaceous deposits partially cemented by clayey siltstone interbedded with
209 thin sand beds that contain saline water (Klausing and Lohman 1964). The overall
210 transmissivity of the siltstone unit is exceptionally low.
211 • The late Pliocene to Holocene reduced clay, silt, and sand green to gray lacustrine and
212 flood-plain deposits have maximum thicknesses of 1000 m in the west (Frink and Kues,
213 1954; Davis et al., 1959, Inter-Agency Committee 1958: Lofgren and Klausing, 1969).
214 Plants and disseminated iron sulfide are well-preserved in them and their saline water is
215 not suitable for drinking or agricultural uses (Lofgren and Klausing, 1969).
216 • The Holocene oxidized continental alluvial deposits are yellow to brown highly
217 weathered sand, silt, and sandy clay feldspar grains (Frink and Kues, 1954; Davis et al.,
218 1959, Inter-Agency Committee 1958: Lofgren and Klausing, 1969). The thickness of
219 these highly weathered sediments is 90-200 m, and the unit is overlaid by 60-80 m of
220 slightly weathered, highly calcareous permeable alluvial deposits. These calcareous
221 deposits represent a time-lapse and a transition in the weathering regime (Lofgren and
222 Klausing, 1969), and constitute the principal aquifer in the study area.
223 • The Corcoran Clay deposits are silty clay to clayey silt diatomaceous Pleistocene deposits
224 occupying half of the study area in the western side. They are principal confining
225 formation beneath the alluvial deposits and flood plain with thicknesses ranging from 0 m
226 in the east to more than 30 m in the west (Lofgren and Klausing, 1969).

227 The regional groundwater flow is from east to west, following the Sierra Nevada streams. The
228 oxidized alluvial deposits form the principal unconfined aquifer in the eastern part of the study
229 area transitions to semiconfined and confined aquifers in the west because of the Corcoran Clay.
230 In the east, the saline water has naturally been replaced by fresh water forming a secondary
231 confined aquifer in the Santa Margarita Formation. The low-quality high salinity groundwater is
232 in the western part of the confined Pliocene sediments aquifer and the confined Santa Margarita
233 Formation aquifer (Lofgren and Klausing, 1969).

234 **2.3. Hydrochemical and Isotopic Data**

235 We used hydrochemical and isotopic data from domestic wells sampled as part of the US
236 Geological Survey (GAMA) Program (Bennett et al., 2017). The dataset includes 95 wells
237 sampled from November 2014 to April 2015. Among multiple groundwater-quality parameters,

238 we used pH, temperature (T), alkalinity, major ions (Ca, Mg, Na, K, Cl, SO$_4$), NO$_3$, Br, stable
239 isotopic ratios of hydrogen (^{2}H), oxygen (^{18}O), and carbon (^{13}C), and tritium (^{3}H). The quality
240 criterion for the chemical analyses was cation-anion imbalances of $\leq$ 10%. Unfortunately, only
241 40% of the wells (41 wells) had ion imbalance errors of smaller than 10%, and the remainder (54
242 wells) had higher errors and were discarded from the chemical analysis. These 54 wells were
243 included for pH, temperature, stable hydrogen (^{2}H), oxygen (^{18}O), and tritium (^{3}H)
244 analysis. Rainwater isotopic content was obtained from previous studies in California (Visser et
245 al., 2018; Friedman et al., 1992; Rose et al., 1996). Meltwater isotopic signatures were from a 2-
246 year study in the Marble Fork of the Kaweah (Figure 1a) watershed (Huth et al., 2004).

247 The studied groundwater system was divided into four aquifer regions. The Mountain Range
248 Aquifer (MRA) includes 18 wells at 181 to 876 m elevations with depths varying from 30 to 182
249 m. The Upper Valley Aquifer (UVA) comprises the unconfined regions of the Central Valley
250 aquifer and includes 37 wells at elevations from 61 to 149 m and depths of less than 100 m (17-
251 98m). The Lower Valley Aquifer (LVA) comprises the semi-confined to confined areas of the
252 Central Valley aquifer and includes 23 wells with depths greater than 100 m (107-453 m) and
253 elevations from 64 to 214 m. The 100 m separation depth for differentiating UVA from the LVA
254 was based on the geological cross-section A-A' (Figure 2a) of Lofgren and Klausing (1969) and
255 was confirmed by a recent large-scale geophysical investigation (Kang et al., 2022). This
256 division was not applied to the Western Valley Aquifer (WVA) wells close to the historical
257 Tulare Lake. Elevation of the 15 WVA wells ranges from 66 to 81 m, with depths from 24 to
258 91m. Nearly all shallow wells are pumping fresh water from the continental oxidized alluvial
259 deposits. Only WVA and western LVA wells are extracting water from the continental lacustrine
260 deposits. Eastern LVA wells are pumping freshwater from saline Tertiary deposits which saline
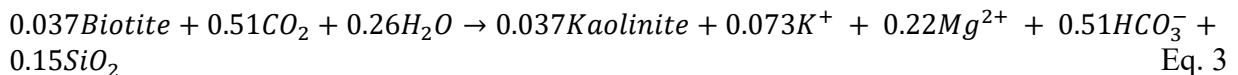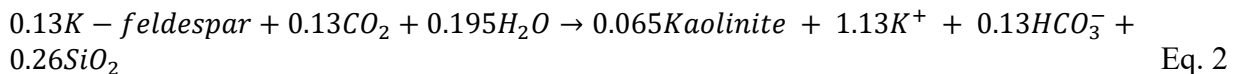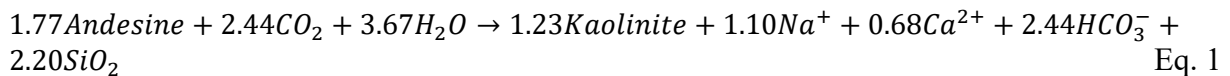261 formation water has been flushed out.

2.4. Isogeochemical Analysis and Modeling

262

263   2.4.1. Characterizing Chemical and Stable Carbon (^{13}C) Isotopic Signatures of the Mountain-
264   Valley Aquifer system

265 We employed a multi-tool approach using hydrochemical data to determine groundwater
266 chemical facies of aquifers. After identifying temperature and pH ranges of wells, groundwater
267 chemical facies were determined by Stiff diagrams. The potential processes driving each facie
268 were determined using a Piper diagram and later validated using multiple approaches. The
269 influence of evaporation and cation exchange processes were evaluated using two models built in
270 PHREEQC version 3 (Parkhurst & Appelo, 2013). In the first model, evaporation was the main
271 process driving dissolved cations in the MRA. The evaporation effect was assessed by
272 calculating a concentration factor (C$_f$) using the Giant Forest Rain station data in the Kaweah
273 River watershed (Figure 2a) (NADP, 2022). Assuming Cl was conservative, the C$_f$ was obtained
274 by comparing the average Cl concentrations in the MRA groundwater and volume-weighted
275 precipitation accounting for wet and dry deposition from the 1980-2020 period. In the second
276 model, evaporation and cation exchange were considered. The average exchangeable base
277 concentrations were obtained using soil information from two sites in the Tokopah Watershed
278 located in the Kaweah River basin (Figure 2a) (Table S1). The average exchangeable base
279 concentrations were converted from meq/100g to eq/kg using sediment porosity of 0.45 and soil
280 bulk density of 2.6 g/cm^3. Exchange equilibrium constants were from Appelo & Postma (2005)
281 following the Gaines-Thomas convention. The plausibility of both models was assessed by

282 comparing the estimated dissolved cations concentrations to the average measured concentration
283 in the MRA.

284 While evaporation and cation exchange primarily relate to soil driven processes within the
285 unsaturated zone, groundwater chemistry is highly influenced by mineral dissolution and
286 precipitation processes. These processes were evaluated using mineral saturation indices (SI). SI
287 indicates how far groundwater is from the mineral equilibrium and determines the dissolution or
288 precipitation potential of a specific mineral. SI was computed with PHREEQC using in-situ
289 temperature, pH, and alkalinity measurements. Mineral equilibrium was assumed within ± 0.5 of
290 SI. Complementary to the SI, mineral dissolution was assessed by bivariate analysis of
291 groundwater dissolved solutes. The bivariate analysis of reaction products is instrumental when
292 dissolution and precipitation processes cannot be identified by the SI. For example, as silicate
293 dissolution is slow, silicates are expected to be far from equilibrium indicating sub-saturation. In
294 addition, silicates are usually altered to other minerals with a different chemical structure and
295 composition. A well-known example is weathering of the Sierra Nevada granite studied by Feth
296 et al. (1964) and Garrels and McKenzie (1967). In these studies, granite silicates including
297 andesine $Na_{0.62}Ca_{0.38}Al_{1.38}Si_{2.62}O_8$, K-feldespar and biotite $KMg_3AlSi_3O_{10}(OH)_2$ were altered
298 to kaolinite $Al_2Si_2O_3(OH)_4$, releasing Na^+, Ca^{+2}, K^+, HCO_3^- and SiO_2 as follows:

299 $1.77 Andesine + 2.44CO_2 + 3.67H_2O \rightarrow 1.23 Kaolinite + 1.10Na^+ + 0.68Ca^{2+} + 2.44HCO_3^- +$
300 $2.20SiO_2$ Eq. 1

301 $0.13K - feldespar + 0.13CO_2 + 0.195H_2O \rightarrow 0.065 Kaolinite + 1.13K^+ + 0.13HCO_3^- +$
302 $0.26SiO_2$ Eq. 2

303 $0.037 Biotite + 0.51CO_2 + 0.26H_2O \rightarrow 0.037 Kaolinite + 0.073K^+ + 0.22Mg^{2+} + 0.51HCO_3^- +$
304 $0.15SiO_2$ Eq. 3

305 Bivariate analysis was fundamental to understand water-rock reactions in the aquifer systems.
306 Moreover, it was used to identify: (1) pollution from the agriculture fields through the NO_3-SO_4
307 relation, and (2) seawater mixing from the Tertiary marine deposits through the Na-Cl and SO_4-
308 Cl relations.

309   2.4.2. Characterizing MSR Processes with Stable Oxygen (^{18}O) and Hydrogen (^{2}H) Isotopes
310   and Tritium (^{3}H)

311 Stable [18]O and ^{2}H groundwater isotopes were used to differentiate focused from diffuse MAR in
312 the MRA wells. Focused MAR mainly occurs via streamflow infiltration and seepage from lakes
313 through the mountain block, and groundwater samples are expected to express isotopic
314 fractionation due to evaporation. Stable isotopic data from the evaporated MRA wells
315 representative of focused MAR in the Sierra Nevada were used to build a Local Evaporation
316 Line (LEL). To identify recharge sources (rain, snowmelt, and surface water) in the MRA wells,
317 stable isotopic values of fourteen MRA wells located in four different transects across the
318 elevation gradient (Figure 2a) were used.

319 The MFR was attributed to shallow wells at the mountain front with the isotopic signature of
320 evaporated Sierra Nevada rivers (focused MAR) and the chemical signature of unsaturated zone
321 processes. The deep MBR was attributed to deep wells with the chemical signature of water-
322 granite reactions and long residence times (tritium concentrations are ≤0.5 tritium units (TU)).

323

2.4.3. Quantifying the Connectivity between the Mountain and Valley Groundwater Systems

The proportion of MFR and MBR in valley aquifer wells was computed using the (1) End-Member Mixing Analysis (EMMA) (Christophersen and Hooper, 1992; Hooper, 2003) and (2) mixing ratio calculation (MIX) (Carrera et al., 2004). EMMA is based on the principal component analysis, aiming to find the composition and a minimum number of end-members needed to explain the variability of measured concentrations within water samples. MIX calculates the mixing ratios of the identified end-members in each sample using the concentrations of conservative species. A detailed description of MIX can be found in Carrera et al. (2004), and a summary is provided below. The mass balance equation of a sample (mixture) p for species s is defined as (Carrera et al., 2004):

$$y_{ps} = \sum_{e-1}^{ne} \delta_{pe} x_{es} + \varepsilon_{ps} \qquad where\ s = 1, ..., ns \qquad \text{Eq. 4}$$

Where y_{ps} and x_{es} are the concentrations of species s in sample p and end-member e, respectively, δ_{pe} is the proportion of end-member e in mixture p, and ε_{ps} accounts for measurement and conceptual errors caused by the non-constant concentration of an end-member. When the end-member concentrations are known, the errors in simulated concentrations can be calculated using an objective function.

Correct application of EMMA and MIX requires selection of conservative species, and end-members with significant differences in species concentrations (Christophersen and Hooper, 1992; Hooper, 2003; Carrera et al., 2004; Barthold et al., 2011). As achieving conservative condition due to water-rock reactions in groundwater is challenging (Parkhurst, 1997; Carrera et al., 2004), we followed the Pelizardi et al. (2017) approach by linearly combining non-conservative species with conservative chemical components. Components are linear combinations of species that remain unchanged by reactions. For example, the component $U_{gypsum} = Ca^{+2} - SO_4^{-2}$ will not change by gypsum dissolution (Eq. 5), and the exact amount of Ca^{+2} and SO_4^{-2} release by gypsum dissolution is predicted by:

$$CaSO_{4(s)} \leftrightarrow Ca^{+2} + SO_4^{-2} \qquad \text{Eq. 5}$$

Therefore, subtracting the molar concentration of SO_4^{-2} from Ca^{+2} will always give the same result, maintaining U_{gypsum} constant. In order to build chemical components, the chemical reactions and species must be defined in a stoichiometric matrix (Eq. 6), and components are built following Eq. 7.

$$S = N_r \times N_s \qquad \text{Eq. 6}$$

$$U = (N_s - N_r) \times N_s \qquad \text{Eq. 7}$$

Where S is the stoichiometric matrix containing the stoichiometric coefficients of the reactions, N_r is the number of reactions, N_s is the number of species, and U is a component. A detailed description of the component and stoichiometric matrices can be found in Molins et al. (2004) and Pelizardi et al. (2017), respectively. We also used components to validate processes

368   identified in Section 2.4.1. In EMMA, changes in species concentrations are presented via
369   eigenvectors. Therefore, an eigenvector accounts for gypsum dissolution would contribute to
370   Ca^{+2} and SO_4^{-2} in the same direction, either positive or negative, and the contribution will be the
371   same due to the stoichiometry of Eq. 1 and range from 0 to 1. In general, more eigenvectors
372   explain more variance of the sample composition as more species are considered.
373
374   In this study, end-members are representative samples of each main chemical groundwater type
375   associated with MSR processes. A number of EMMA models were developed using different
376   end-members, solutes, isotope tracers, and chemical reactions. The variance, R^2, and root mean
377   squared error (RMSE) were jointly used to determine the best model (i.e., the model with the
378   highest variance and the best fit between measured and modeled concentrations). Slope (m)
379   identified the direction of those differences. Finally, the best-performing EMMA model was
380   selected to run with MIX to obtain the percentage of MSR processes in each well, and quantify
381   the connectivity between the mountain and valley groundwater.
382

383   **3.   Results and discussion**

384   **3.1. Characterizing Chemical and Stable Carbon (^{13}C) Isotopic Signatures of the**
385   **Mountain-Valley Aquifer system**

386   The average groundwater temperature in the study area is 20°C. Temperature ranges are 17 –
387   23°C (average = 20°C) in the MRA wells, and the UVA wells, 19 – 28°C (average= 23°C) in the
388   LVA wells, and 19 to 23°C (average= 20°C) in the WVA wells. Only the LVA samples are three
389   degrees warmer than the average groundwater temperature (Figure 3c). pH ranges in the MRA
390   are 6.1 to 7.8 (average = 6.9), 6.9 to 8.5 (average= 7.6) in the UVA wells, 7.1 to 8.4 (average=
391   8.0) in the LVA wells, and 7.2 to 9.1 (average= 7.7) in the WVA wells (Table S1). On average
392   the MRA wells (pH= 6.9) have lower mean pH than the study area average (pH= 7.7), indicating
393   newly recharged groundwater with pH values closer to the average rainwater (pH ~ 5.5 for the
394   1980-2020 period). The LVA samples have a slightly higher pH and temperature (on average
395   3°C warmer than other regions) suggesting longer residence time.

396   Stiff diagrams indicate the presence of two major and three minor chemical facies (Figure 3a).
397   Major groundwater types are Ca-HCO$_3$ and Na-HCO$_3$ as HCO$_3$ is the dominant anion of the
398   entire dataset. In some samples (n=6, Figure 3a) SO$_4$ and HCO$_3$ are similar, leading to the minor
399   chemical facie Na-HCO$_3$SO$_4$. Higher dissolved Cl concentration relative to HCO$_3$ in five
400   samples results in two additional minor chemical facies, Na-Cl and Ca-Cl groundwater types.
401   These wells are KAW04 in the UVA, TLE03 in the LVA, and TLA13, 14, and 15 in the WVA
402   (Figure 3a). Cl only increases in a few samples (arrow c in Figure 3b) suggesting the influence of
403   local processes driving Cl concentration. In contrast, SO$_4$ increases without exceeding HCO$_3$
404   (arrow *b* in Figure 3b) in all the aquifer regions except the MRA suggesting the role of regional
405   processes on SO$_4$ concentrations.

406   Regarding the cations, the Ca-HCO$_3$ groundwater type dominates MRA and UVA regions except
407   for 1 out of 10 (HLS14, Figure 3a), and 5 out of 16 Na-dominated samples. In the LVA and
408   WVA regions, groundwater has evolved to Na-HCO$_3$ except for 4 out of 12 Ca-dominated
409   samples in the LVA, and one Ca-Cl sample in the WVA (TLA13, Figure 3a). The Ca-HCO$_3$

410 evolved to Na-HCO$_3$ (arrow (a) in Figure 3b) while sulfate increases (arrow (b) in Figure 3b)
411 suggesting the role of regional processes on groundwater evolution.
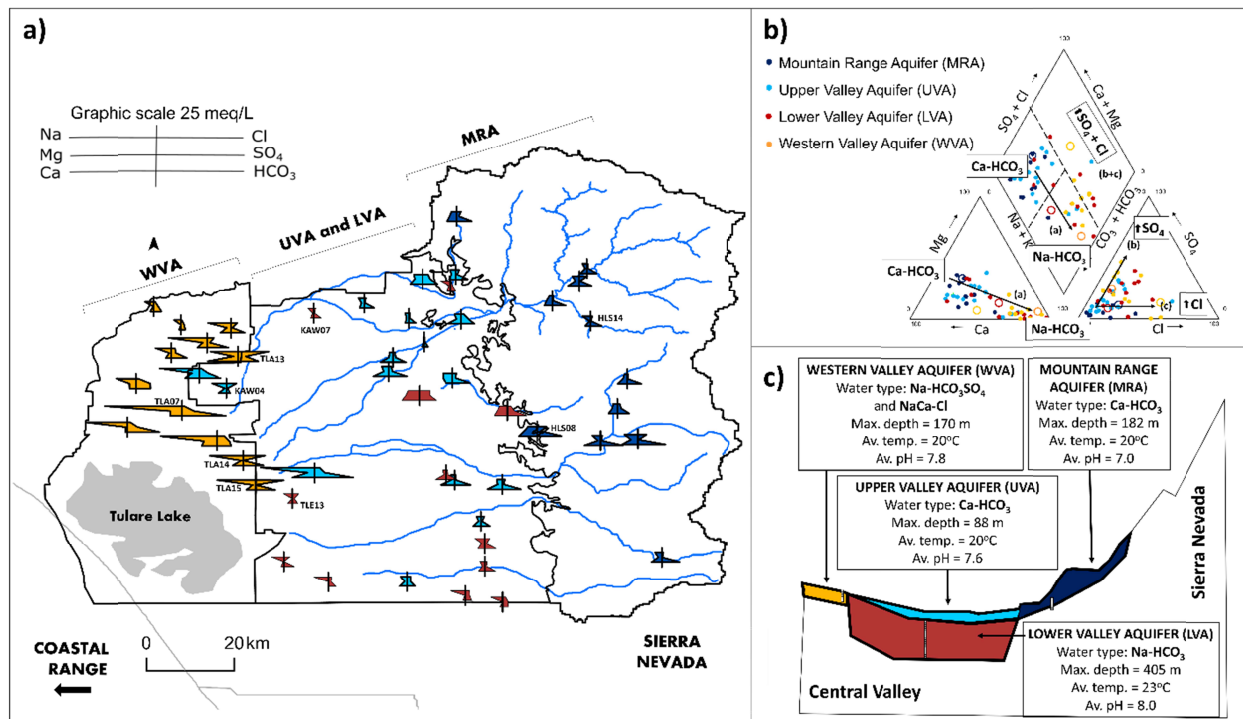
Figure 3 a) Spatial distribution of the Stiff diagrams. Each groundwater region is presented with a different color (MRA: dark blue, UVA: light blue, LVA: red, WVA: orange). B): Projection of the major chemical component of groundwater samples on a Piper diagram. Arrows highlight the main observed trends in groundwater chemistry. The empty circles are the selected end-members for the MIX analysis. C) Main hydrochemical features of each groundwater region.

418 3.1.1. Processes Driving the Major Ion Evolution in the Mountain-Valley Aquifer Regions

419 <u>Mountain Range Aquifer</u>

420 The Ca-HCO$_3$ groundwater type of the MRA was previously reported for the vast majority of
421 Sierra Nevada rivers and lakes (White et al., 1999; Melack et al., 1985; Melack et al., 2020). This
422 similarity with the surface water chemistry and rainwater pH suggests that the Ca-HCO$_3$
423 groundwater type represents newly recharged groundwater in the Sierra Nevada and its
424 chemistry is likely influenced by soil-related processes such as evaporation and cation exchange.
425 To evaluate this hypothesis two models that consider evapoconcentration and cation exchange
426 processes are developed (Table 1). Model A accounts for increases in dissolved solutes due to
427 evaporation and computes a concentration factor (C$_f$) using the rainwater and MRA samples by
428 assuming Cl as a conservative solute. The ratio of average Cl concentration in the MRA (34.3
429 mg/L) and rainfall (0.11 mg/L) results in C$_f$ of 311. The high evapoconcentration factor agrees
430 with the significant mean evapotranspiration rate for the 1982-2019 period in the Mountain
431 Range (639 mm/yr) (Elnashar et al., 2020) accounting for 84% of the average rainfall (756
432 mm/y) for the same period (NOAA, 2022). Model B considers evaporation and cation exchange
433 processes using the averaged cation exchange capacity (CEC) of two soil types (1.19x 10^{-4}
434 eq/kgw) in the Tokopah watershed (Figure 2a), the exchange equilibrium constants from Appelo
435 & Postma (2005), and following the Gaines-Thomas convention. Model results indicate that the

12

436 amount of cations released in Model B is less than Model A that only considers
437 evapoconcentration. However, evapoconcentration only accounts for 40% of dissolved Ca in
438 MRA groundwater, and other processes such as calcite dissolution and silicate weathering should
439 be considered.

441 **Table 1**. Average chemical composition of the volume-weighted average rainfall at the Giant Forest Rain station
442 during the 1980-2020 period (first row), and average cation and Cl concentrations in the MRA region (mg/L).
443 Calculated cation and Cl concentrations from Model A and B by considering evapoconcentration, and
444 evapoconcentration and cation exchange processes, respectively.

	Ca	Mg	K	Na	Cl
VWA Rainfall (1980-2020)	0.05	0.01	0.02	0.06	0.11
Mean MRA samples	60.0	16.8	4.2	39.10	34.30
Model A – Evapoconcentration	14.36	3.52	5.79	19.91	34.30
Model B – Evapoconcentration + Cation Exchange	10.96	2.05	9.17	24.59	34.30

447 The contribution of calcite dissolution to Ca concentration in surface water bodies and shallow
448 groundwater in the Sierra Nevada is controversial. Some studies demonstrated that more than
449 half of Ca in surface water is released by calcite dissolution (Mast et al. 1990; Clow et al. 1997).
450 A recent study also showed that isolated small karst systems in the Sequoia National Park
451 contribute to 65-86% of baseflow in the North and East Fork of the Kaweah River during the dry
452 season, leading to increases in Ca (Tobin and Schwartz, 2020). White et al. (1999) attributed Ca
453 concentration in the Northern Sierra Nevada groundwater to accessory calcite in fresh granitoid
454 rocks, and Garrels and Mackenzie (1967) attributed 70% of Ca variability in the perennial
455 springs to calcite dissolution and the remainder to evapoconcentration. Other studies indicated
456 that silicate weathering is the main source of Ca (Feth et al., 1964; Wahrhafting, 1965; Melack et
457 al., 2021; Williams et al., 1990; Williams et al., 1993). Among the main Sierra Nevada
458 granodiorites, andesine, quartz, K-feldspar, and biotite, only andesine has the potential to release
459 Ca in groundwater (Feth et al., 1964; Garrels and Mackenzie, 1967; Sisson et al., 1984; Clow et
460 al., 1996). However, andesine weathering cannot solely explain high Ca concentration. Andesine
461 has a molar Ca/Na ratio of <1. Figure 3a shows that Na increases due to andesine weathering are
462 associated with decreases in CO_2 as expected by Eq. 2. (Table S2). Ca/Na ratio of surface water
463 and shallow groundwater of the Sierra Nevada is greater than 1, so andesine is the primary
464 source of Na.

465 Although andesine is the most prevalent silicate in the Sierra Nevada, biotite is the most easily
466 weathered silicate, and about 1%-2% of the biotite is altered to clay minerals (Wahrhafting 1965;
467 Meade 1967). Therefore, biotite weathering and evaporation are the likely sources of dissolved
468 Mg in groundwater (Eq. 6), and silicate weathering and calcite dissolution are sources of Ca and
469 Na in the MRA groundwater. Silicate weathering and calcite dissolution reactions also account
470 for groundwater alkalinity as shown by the HCO_3 release in Eq.1, Eq.2, Eq.3, Eq.4, and Eq.8.

471 $$CaCO_3 + CO_2 + H_2O \leftrightarrow Ca^{+2} + 2HCO_3^-$$ Eq. 8

473 In summary, andesine is the primary source of Na in the MAR, and biotite and evaporation are
474 the sources of Mg. The primary source of K seems to be evaporated rainfall, even though biotite

475 could also contribute. Calcite dissolution releases part of the dissolved Ca and HCO_3 in
476 groundwater, and jointly with silicate weathering contribute to dissolved HCO_3. In agreement
477 with the previous investigations, most of the MRA groundwater samples are in equilibrium with
478 calcite except for a few sub-saturated samples (Figure 3b).
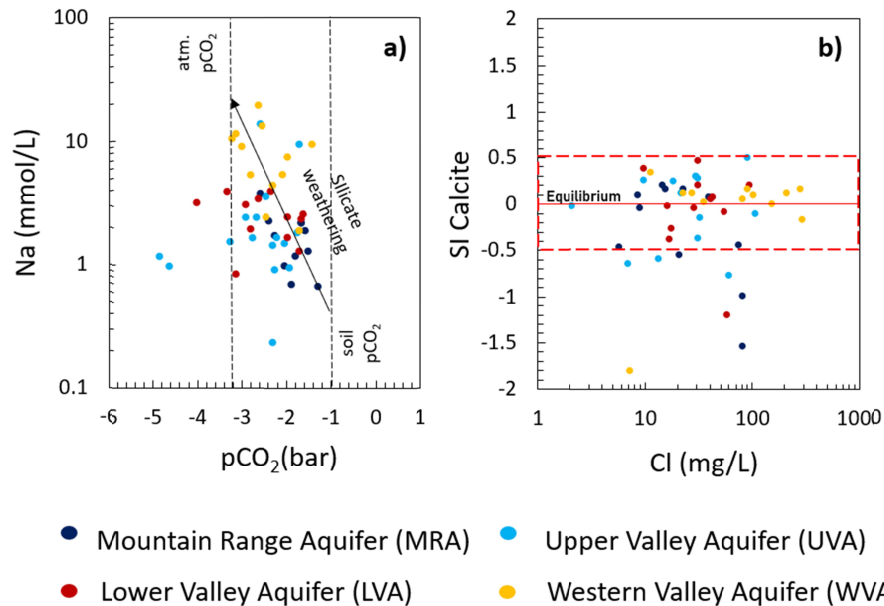
Figure 4. a) Relation between dissolved Na (mmol/L) and dissolved edaphic CO_2 (pCO$_2$ bar); b) Relation between
the SI of calcite ($CaCO_3$) and dissolved Cl (mg/L).

Valley Aquifer System

483 The valley area comprised of UVA, LVA, and WVA groundwater regions. Due to low
484 precipitation in the valley area, valley groundwater is mainly recharged by MFR and MBR
485 processes originating from the mountain and influencing groundwater chemistry of the valley
486 (Figure 1).

487 The Ca-HCO_3 chemical facie of the MRA is also dominant in the UVA region, and highly
488 calcareous alluvial sediments of the UVA (Lofgren and Kalusing, 1969) support calcite
489 dissolution. Calcite equilibrium is achieved in most of the UVA samples (Figure 4b), and calcite
490 equilibrium in the less mineralized samples suggests that the Ca-HCO_3 groundwater type is
491 influenced by soil processes, and rivers and lakes chemistry. The similarity between the MRA
492 and UVA samples implies that unsaturated zone processes impact recharge chemistry.

493 The main differences in the groundwater chemical composition between the MRA, UVA (Ca-
494 HCO_3), and LVA (Na-HCO_3) is the Na dominance among other cations and decreases in
495 dissolved Ca and HCO_3 in the LVA region. The Na dominance suggests strong influence of
496 andesine weathering over calcite dissolution and cation exchange. Andesine weathering is a slow
497 process where thermodynamic equilibrium is rarely attained (Appelo & Postma, 2005).
498 Therefore, long water-rock contact and residence time result in the Na-HCO_3 chemical type. This
499 hypothesis also agrees with the low mineralization of the deepest wells in the LVA (i.e., smaller
500 Stiff diagrams in Figure 3a) region and warmer temperature of the LVA samples due to
501 geothermal characteristics of deep flow circulation (Figure 3c).

14

502 The WVA chemical composition is very similar to the LVA but more mineralized (Figure 3a).
503 The most prevalent solutes in the WVA are Na, HCO_3, SO_4, and Cl (Table S1), resulting from
504 similar water-rock reactions. More mineralization compared to the LVA is consistent with a
505 longer distance from the recharge area (Figure 3c). Another major difference between these
506 regions is the local dominance of Cl over HCO_3. Fuji and Swan (1995) attributed the Cl increase
507 to the influence of Miocene marine sedimentary rocks derived from the Coast Range, seawater
508 mixing, salts dissolution, and evaporative processes. We developed a binary mixing model to
509 explore the possible mixing of fresh groundwater with seawater (Figure 5a). The less mineralized
510 MRA Ca-HCO_3 groundwater sample was selected as the representative freshwater end-member,
511 and the chemical composition of standard seawater was obtained from Hem (1985). The short
512 distance of Na-Cl and Ca-Cl WVA labeled samples from the mixing line suggests that seawater
513 mixing is the main contributor to dissolved Cl (Figure 5a). In Fuji and Swan (1995), evaporation
514 and dissolution of evaporative salts were supported by the observed salt crusts in soils of non-
515 irrigated fields. Salt dissolution potential due to evaporative processes was evaluated by plotting
516 the SI of halite (NaCl) versus Cl (mg/L) (Figure 5b). Results show sub-saturation of halite in all
517 samples, eliminating salt dissolution as the Cl source. Therefore, the dominant processes driving
518 the high mineralization of the WVA region and the local increase in dissolved Cl are prolonged
519 water-rock interactions promoting silicate weathering and mixing with seawater from the
520 Quaternary lacustrine and flood-plain deposits.

521
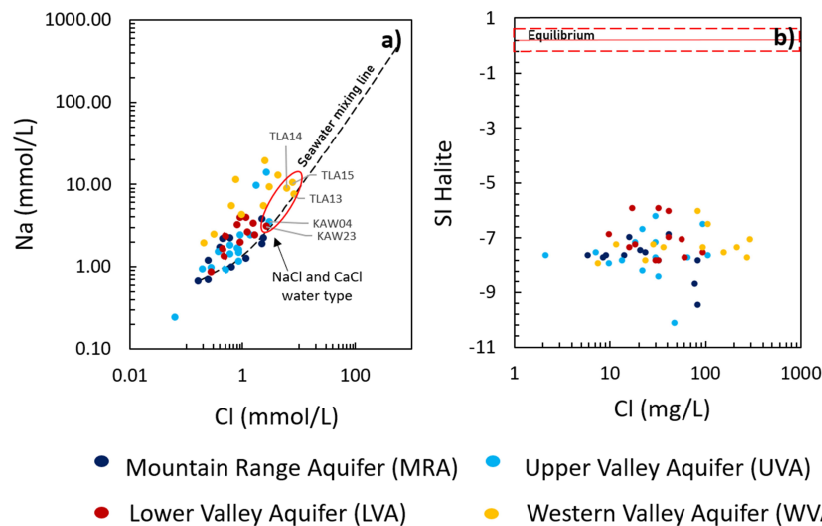
522 **Figure 5**. a) Relation between dissolved Na and dissolved Cl (mmol/L). b) Relation between the SI of halite (NaCl)
523 and dissolved Cl (mg/L).

3.1.2. Assessing Sulfate Sources in Groundwater Samples

525 In all aquifer regions, increases in sulfate are observed (arrow (b) in Figure 3b). The WVA
526 samples have higher dissolved SO_4 concentrations, on average 50 to 85 mg/L more than the other
527 aquifer regions (Table S1). Three potential processes were assessed to explain dissolved SO_4
528 sources: (1) agricultural or sewage contamination, (2) mixing with seawater trapped in the
529 Quaternary and Tertiary sediments, and (3) gypsum dissolution. Agricultural or sewage pollution
530 impact groundwater via direct infiltration of excess fertilizer. Nitrate concentrations in shallow
531 domestic wells in the Central Valley are derived from multiple anthropogenic sources (manure,
532 synthetic fertilizer, and septic/wastewater discharge) (Moran et al., 2011). Therefore, a strong

533 linear relationship between SO_4-NO_3 will suggest SO_4 anthropogenic pollution. However, no
534 correlation (R^2=0.01) between the SO_4 and NO_3 concentrations is found eliminating
535 anthropogenic sources for SO_4 (Figure 6a).
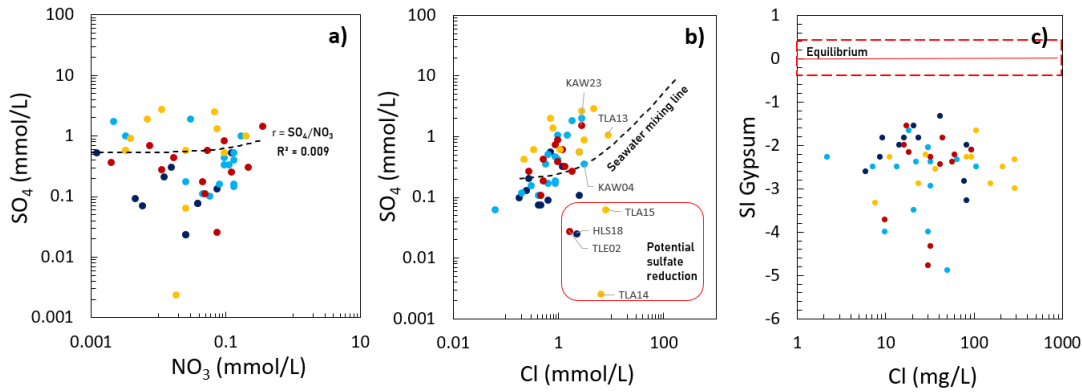
● Mountain Range Aquifer (MRA) ● Upper Valley Aquifer (UVA) ● Lower Valley Aquifer (LVA) ● Western Valley Aquifer (WVA)

536

Figure 6. a) Relation between dissolved SO_4 (mmol/L) and dissolved NO_3 (mmol/L). b) Relation between dissolved
538 SO_4 and dissolved Cl (mmol/L). Labeled samples are Na-Cl, Ca-Cl groundwater type. C) Relation between the SI of
539 gypsum ($CaSO_4$) and dissolved Cl (mg/L).

540 Seawater mixing was evaluated through the mixing model. Most groundwater samples including
541 the Na-Cl dominated samples (labeled samples in Figure 6b) are plotted higher than the Cl-SO_4
542 seawater mixing line indicating higher dissolved SO_4 than expected by the seawater mixing
543 (Figure 6b). Higher SO_4 concentrations in KAW23 and TLA13 samples are related to gypsum
544 dissolution. The Ca-Cl samples have lower SO_4 values than expected by the seawater mixing,
545 potentially due to sulfate reduction processes. Only KAW04 sample seems to be affected by the
546 seawater mixing. Therefore, even if seawater mixing is responsible for higher dissolved SO_4 in
547 some samples, other processes are the main drivers of SO_4 concentration in groundwater.

548 Gypsum dissolution was evaluated by computing the gypsum Saturation Index (SI_{gypsum}). Results
549 shows that all groundwater samples are sub-saturated. Saturation indices of the MRA samples
550 are higher than average (average SI_{gypsum}=-2.1) (Table S2), but small differences are observed
551 among the UVA (SI_{gypsum}=-2.8), LVA (SI_{gypsum}=-2.7), and WVA (SI_{gypsum}=-2.5) samples (Table
552 S1). Feth et al. (1964) reported sulfate nearby fault zones in the Sierra Nevada. In addition,
553 Lofren and Klausing (1969) and Meade (1967) reported sulfate and ion sulfides in the
554 Quaternary sediments. Petrographic evidence suggests that part of the sulfate from the iron
555 sulfide oxidation reacts with calcite forming gypsum in the Quaternary sediments (Meade 1967).
556 The absence of chloride in sediments agrees with our results that the SO_4 increase is not followed
557 by a dissolved Cl increase (Figure 6b). Although gypsum equilibrium is not observed in our
558 samples, gypsum dissolution is likely to occur locally at the fault zones and valley sediments
559 explaining the wide range of dissolved SO_4 in groundwater. However, sulfur isotope analysis is
560 needed to confirm this hypothesis.

561 The evolution of $\delta^{13}C$-HCO_3(‰) in groundwater is used to evaluate the gypsum dissolution
562 hypothesis. Gypsum dissolution ($CaSO_4$) increases dissolved Ca without changing $\delta^{13}C$ (‰)
563 content in groundwater. However, calcite ($CaCO_3$) dissolution results in less depleted $\delta^{13}C$ (‰)
564 values (i.e., $\delta^{13}C$ of calcite is close to 0 ‰).

16
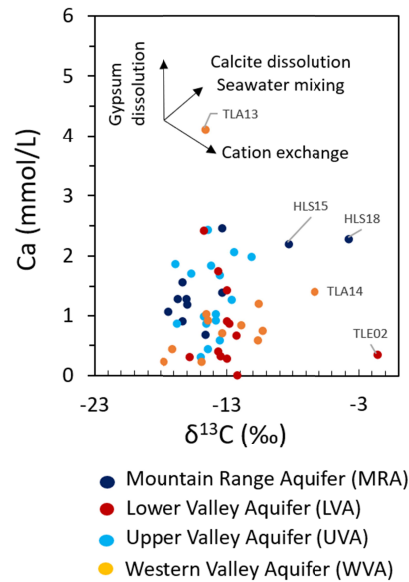
Figure 7. Relation between dissolved Ca (mmol/L) and $\delta^{13}C$ (‰).

Results in Figure 7 confirm that gypsum dissolution drives dissolved Ca concentration in groundwater as groundwater samples follow the gypsum dissolution direction, with some samples having exceptionally high dissolved Ca. The $\delta^{13}C$ (‰) of dissolved inorganic carbon in groundwater samples ranges from -17.16 ‰ to -10.40 ‰, excluding those with anomalous values HLS15, TLA14 HLS18, and TLE02 samples (-8.4‰ < $\delta^{13}C$ < -1.68 ‰). Dissolved inorganic carbon in the above samples with larger $\delta^{13}C$ (‰) values is usually the result of organic matter oxidation. In this case, sulfate reduction is likely oxidizing the organic matter and driving increases in $\delta^{13}C$ values due to the low dissolved SO_4 (Figure 6 and Table S2). Additionally, calcite dissolution locally enhanced by Ca-Na cation exchange seems responsible for the $\delta^{13}C$ of -17.16‰ to -10.40 ‰ in groundwater. $\delta^{13}C$ of a groundwater system in equilibrium with calcite would range from -16‰ to -12‰. However, some samples have larger $\delta^{13}C$ values due to Ca-Na cation exchange and oversaturation. Finally, gypsum and calcite dissolution are regional processes driving the dissolved Ca, SO_4 and HCO_3 in groundwater and oxidation of organic matter and cation exchange only have local effect.

3.2. Characterizing Chemical and Isotopic Signatures of MSR processes with Stable Oxygen (^{18}O) and Hydrogen (^2H) isotopes and Tritium (^3H)

Groundwater δ^2H and $\delta^{18}O$ values from all four groundwater regions are plotted along the Global Meteoric Water Line (GMWL; Craig, 1961). The isotopic content of the samples ranges from -51.1‰ to -97.4‰ for δ^2H and -5.68‰ to -13.59‰ for $\delta^{18}O$ (V-SMOW) (Figure 8a). A Local Evaporation Line was determined from the MRA region samples (Figure 8a), and its slope agrees with the US rivers (Kendall & Coplen, 2001; Mast et al., 1990).

The slope of the topographic fractionation effect in California ranges from -1.7 to -2.7 ‰ per vertical km for $\delta^{18}O$ ‰ (Friedman, 1992; Rose et al., 1996; Lechler et al., 2012; Visser et al., 2018). However, comparing the expected topographic fractionation with the isotopic composition of samples along the elevation transects (Figure 2a) indicates a different response. While the estimated topographic fractionation effect is 1.15‰ between the $\delta^{18}O$ values of T1 and

593   T4 wells (1062 – 386 = 676 m altitude difference, Figure 8b), the observed difference is 0.42‰
594   (Figure 8b). This result highlights the importance of snowmelt processes in controlling the
595   isotopic composition of meltwater. Accordingly, the $\delta^{18}O$-δ^2H isotopic space was divided by the
596   precipitation type: rainwater versus meltwater while considering different stages of snowmelt.
597   Rainwater isotopic content was obtained from previous studies in California (Visser et al., 2018;
598   Friedman et al., 1992; Rose et al., 1996). Meltwater signatures were from a 2-year study in the
599   Marble Fork (Figure 1a) watershed indicating $\delta^{18}O$ ranges of -16‰ to -14‰ for the initial
600   meltwater and -11‰ to -10‰ for the final meltwater (Huth et al., 2004) (Figure 8a).
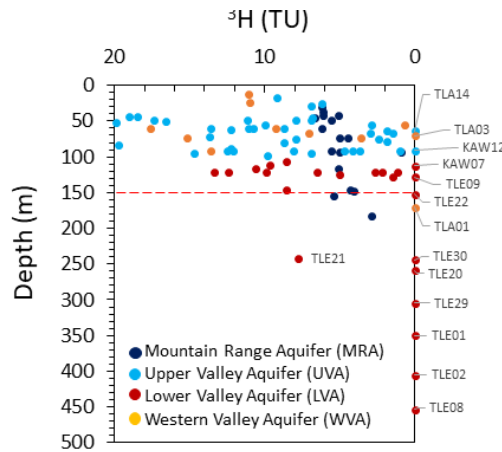
601   The oxygen and hydrogen isotope composition of the MRA wells seems to be influenced by
602   fractionation during snowmelt and evaporation, except for the only Na-HCO$_3$ and non-
603   evaporated MRA sample (HLS14) (Figure 3a). Isotopic values of MRA wells follow the LEL
604   ($\delta^{18}O$ values range from -9.82‰ to -5.68‰) are representative of focused MAR and are
605   comprised of rainwater and final meltwater.

606
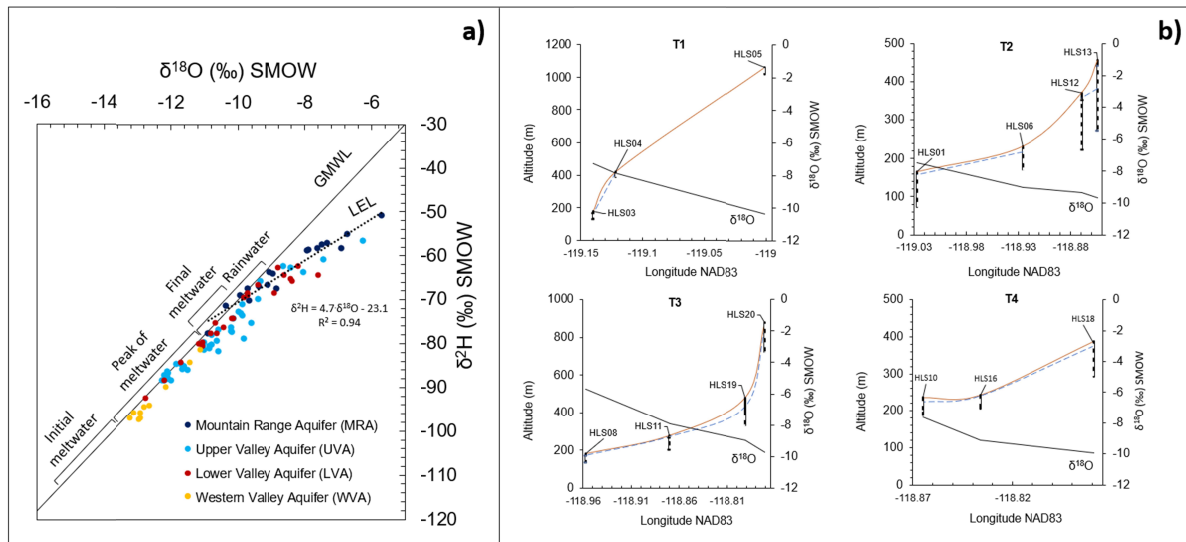
Figure 8. a) δ^2H and $\delta^{18}O$ content in groundwater. Global Meteoric Water Line (GMWL; Craig (1961)) and Local
Evaporation Line (δ^2H =4.6$\delta^{18}O$ -23.3). Initial and final meltwater isotopic ranges are from Huth et al. (2004). Rain
isotopic values are from Visser et al. (2018), Friedman et al. (1992) and Rose et al. (1996). B) Altitude of wells
(orange line), groundwater level (discontinuous blue line), well (black line) and screen depth (discontinuous black
line), and $\delta^{18}O$ values of four MRA transects.

612   The evaporation signature jointly with the Ca-HCO$_3$ groundwater type, characteristic of surface
613   water bodies, are used to identify MFR. UVA groundwater samples located at the mountain front
614   or close to the Kaweah River follow the LEL (KAW18,19,25,26,28,29; TLE23,25,27, Figure 2a)
615   and are Ca-HCO$_3$ type (Figure 3a) indicating MFR influence. The non-evaporated Ca-HCO$_3$
616   UVA samples influenced by soil processes, represent diffuse MAR and shallow MBR recharging
617   the first 100 m of the unconfined aquifer. The LVA groundwater samples from the deeper wells
618   (depth > 150 m) close to the mountain front (TLE20, 22,29,30 Figure 2 and Table S1) also
619   follow the LEL and are mostly Na-HCO$_3$ groundwater type indicating the influence of focused
620   MAR and deep MBR processes. Non-evaporated LVA and all WVA samples following the
621   GMWL represent diffuse MAR and deep MBR processes, and their isotopic signatures indicate
622   the influence of meltwater recharge during the peak of snowmelt (days 170 – 210 of the water
623   year).

624 To further confirm the long residence time of MBR recharging the confined aquifer groundwater
625 tritium (^3H) content was used. Tritium has a half-life of 12.5 yr. implying complete decay (i.e.,
626 tritium units (TU) = 0) after 50 years. Groundwater ^3H content ranges from 20 to 0 TU (Table
627 S1). The LVA and WVA samples from wells with depths greater than 150 m have 0 TU (Figure
628 9) and are Na-HCO$_3$ with the exception of Ca-HCO$_3$ LVA sample (TLE21). These results agree
629 with Visser et al. (2016) that predict 3 to 0 TU in California wells with depths greater than 122
630 m. Wells with depths greater than 150 m and residence times longer than 50 years that contain
631 evaporated Na-HCO$_3$ groundwater type are recharged by focused MAR. This result highlights
632 the contribution of mountain rivers and lakes to confined aquifer recharge. LVA wells with more
633 than 0 TU that have long-screens with the screen top in the unconfined aquifer (Table S1) are the
634 result of mixing with shallower young groundwater. Five UVA wells with depths less than 150
635 m (samples TLA14, KAW12, TLA03, KAW09, and TLE09) have also 0 TU and are Na-HCO$_3$
636 indicating shallow MBR recharge with long residence time. Shallow MBR is a result of complex
637 geology of mountain ranges and presence of faults and fractures impacting flow direction.


638

639 **Figure 9**. Tritium (Tritium Units, TU) content in groundwater samples in the study.

640 In summary, rain and meltwater are sources of recharge. The oxygen and hydrogen isotopic
641 composition of the MRA groundwater is highly influenced by meltwater processes rather than
642 the topographic isotope effect, and focused MAR is the dominant recharge process. Focused
643 MAR is the evaporated Ca-HCO$_3$ water type that recharges the first 100 m of the upper valley
644 aquifer and along with evaporated Na-HCO$_3$ also contributes to deep MBR in the confined
645 aquifer (Figure 10). As a result, groundwater chemistry at the piedmont zone is influenced by
646 focused MAR discharging to valley aquifer and focused MFR from mountain streams. Meltwater
647 from diffuse MAR either becomes Ca-HCO$_3$ water and contributes to shallow MBR in the UVA
648 region (Figure 10), or infiltrates though the saprolite layer, faults and joints, and recharges the
649 deeper aquifer and becomes Na-HCO$_3$ water type that contributes to deep MBR in the LVA and
650 WVA regions (Figure 10). The shallow MBR zone near the foothills represents a mixing zone
651 that consists of Na-HCO$_3$ water type from the LVA region and Ca-HCO$_3$ water type from the
652 UVA region (Figure 10). Evapotranspiration, calcite dissolution, and biotite weathering are
653 responsible for the Ca-HCO$_3$ groundwater, and andesine weathering is responsible for the Na-
654 HCO$_3$ groundwater type. The Na-HCO$_3$SO$_4$ groundwater type is associated with deep MBR and
655 prolonged exposure to silicate weathering and gypsum dissolution in the western region of the

656 upper aquifer. The NaCl and CaCl groundwater types are related to local mixing with connate
657 seawater and are not related to MSR.

658
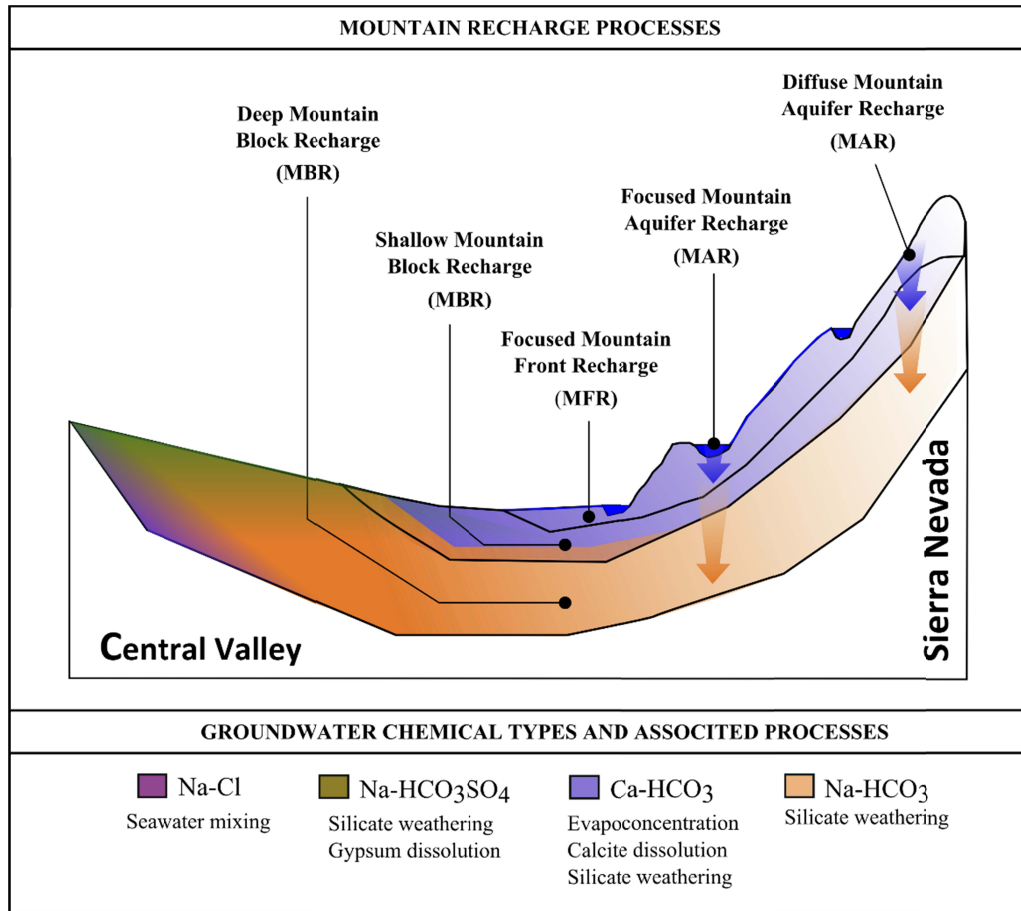
659
660
661 **Figure 10.** Conceptual illustration of the relation between the five recharge pathways in the study area, along with
662 the main groundwater chemical types and their associated hydrogeochemical processes. Chemical groundwater
663 facies are shown in different colors and polygons represent the spatial distribution of MFR, shallow MBR and deep
664 MBR processes.

665

666 **3.3. Determining MBR and MFR Contributions via End-member (EMMA) and MIX**
667 **Analyses**

668 Results of the chemical and isotopic analyses informed end-member selection for the EMMA
669 and groundwater chemistry data are used to determine ratios of MFR and MBR using MIX
670 across the valley aquifer system.

671 3.3.1. End-member and Solutes Selection for EMMA

672 To explain the chemical variability of groundwater, different mixing models were developed to
673 find the best end-members and tracers. These models included different combinations of end-
674 members and tracers, and the model selection was based on the percentage of variance explained
675 by the three eigenvectors (EG1, EG2 and EG3) while ensuring that the projected components
676 were enclosed by the end-member triangle at the EG1-EG2 and EG1-EG3 projection space. For
677 the end-member analysis, two general models with 3 and 4 end-members were developed (Table
678 2). Model 1 consists of an evaporated Ca-HCO$_3$ groundwater type sample (HLS08) from the

679   MRA representing MFR, a 0-Tritium Na-HCO$_3$ sample (KAW07) from the LVA to represent the
680   deep MBR, and a Na-HCO$_3$SO$_4$ groundwater type sample (TLA07) from the WVA representing
681   deep MBR with long exposure to water-rock reactions. In addition to end-members in Model 1,
682   Model 2 includes a Ca-Cl groundwater sample (TLA13) from the WVA representing mixing
683   with connate seawater. This sample is not related to the MSR process. All selected end-members
684   are plotted as empty circles in Figure 3b.

685   In Model 1, the coefficient of determinations between the measured and modeled values of Mg,
686   K, and SO$_4$ are large (R$^2 \geq 0.75$; RMSE ≤ 0.32). However, poor results are obtained for Cl, Na,
687   alkalinity (RMSE ≥ 1.75), Ca, and pH (R$^2 \leq 0.44$). Model 2 results are satisfactory for Mg, K,
688   and pH (R$^2 \geq 0.77$; RMSE ≤ 0.39) and are significantly better than Model 1 for Ca and Cl (R$^2 \geq$
689   0.72; RMSE ≤ 0.6). However, further improvement for estimating Na, alkalinity (RMSE ≥ 1.71),
690   and pH (R$^2 \leq 0.2$) is needed. Differences between measured and modeled concentration are
691   related to overestimation of all solutes, except SO$_4$ (slope, m<1, Table 2). Among all parameters
692   in Model 2, pH was the only one with a non-acceptable R^2 (0.1, Table 2). This result suggests
693   that multiple non-linear reactions could affect pH.

694   To improve Model 2 performance different tracers were added or removed resulting in Model 2a
695   to 2d (Table 2). Removing pH in Model 2a increased the total variance explained by all the
696   solutes by 4% (Table 2). Stable δ^{18}O (‰), δ^2H (‰), and δ^{13}C (‰) isotopes were added in
697   Models 2b, 2c, and 2d, respectively. However, very poor R^2 and RMSE are obtained, and the
698   total explained variance decreased to 79%. EMMA analysis seems inappropriate for identifying
699   evaporation using δ^{18}O (‰) and δ^2H (‰). In addition, poor results for δ^{13}C (‰) and pH are
700   attributed to multiple, non-linear processes, and local processes affecting the C and H$^+$
701   concentrations in groundwater. Finally, Model 2a is selected for the EMMA analysis which only
702   considers the chemical differences among the samples. This means that the evaporated Ca-HCO$_3$
703   end-member is representative of MFR and shallow MBR as it is not possible to distinguish non-
704   evaporated Ca-HCO$_3$.

705   The composition of three eigenvectors (EG) of Model 2a are plotted in Figure 11 and defined by
706   EG1, EG2 and EG3 in EG1-EG2 and EG2-EG3 spaces shown in Figure 12. Positive EG
707   contributions in Figure 11 are related to changes in samples concentrations plotted on the right
708   side of the 0 value in the EG1-EG2 and EG2-EG3 (Figure 12). Negative contributions are related
709   to changes in samples concentration are on the left side of the 0 value.

710   **Table 2.** Results of EMMA analysis: coefficient of determination (R^2), root-mean-squared error (RMSE), slope (m),
711   and total representative variance (%) of major solutes (mol/L), pH and stable δ^{18}O, δ^2H, and δ^{13}C between measured
712   and modeled concentrations for various models. Only subset of models is shown here. *Statistics computed with
713   μmol/L due to low H concentration (<0.001 mol/L) and output format of MIX printing values up to 3 significant
714   digits.

715

| Model	Ca			Na			Mg			K			Cl			Alk			SO$_4$			pH*			δ^{18}O			δ^{2}H			δ^{13}C			Variance (%)
	m	RMSE	R^2	m	RMSE	R^2	m	RMSE	R^2	m	RMSE	R^2	m	RMSE	R^2	m	RMSE	R^2	m	RMSE	R^2	m	RMSE	R^2	m	RMSE	R^2	m	RMSE	R^2	m	RMSE	R^2	
1	0.7	0.7	0.4	0.7	2.4	0.8	0.7	0.2	0.8	0.7	0.03	0.7	0.2	1.8	0.1	0.5	1.9	0.6	0.9	0.3	0.8	0.1	0.1	0.2										82
2	0.7	0.5	0.7	0.7	1.8	0.9	0.7	0.2	0.9	0.8	0.02	0.8	0.9	0.6	0.9	0.6	1.7	0.7	1.2	0.4	0.8	0.1	0.1	0.2										82
2a	0.7	0.5	0.7	0.8	1.9	0.9	0.7	0.2	0.9	0.8	0.00	0.8	1.0	0.6	0.9	0.6	1.7	0.7	1.1	0.4	0.8													86
2b	0.8	0.5	0.7	0.8	1.6	0.9	0.8	0.2	0.9	0.8	0.00	0.8	0.9	0.6	0.9	0.6	1.7	0.7	1.1	0.4	0.8				0.4	1.4	0.4							80
2c	0.7	0.5	0.7	0.8	1.7	0.9	0.7	0.2	0.8	0.8	0.00	0.8	0.9	0.6	0.9	0.6	1.7	0.7	1.1	0.4	0.3							0.4	9.1	0.4				81
2d	0.6	0.6	0.7	0.8	1.7	0.9	0.6	0.3	0.8	0.6	0.00	0.6	0.8	0.6	0.9	0.5	1.8	0.7	1.0	0.3	0.8										0.4	5.5	0.1	79
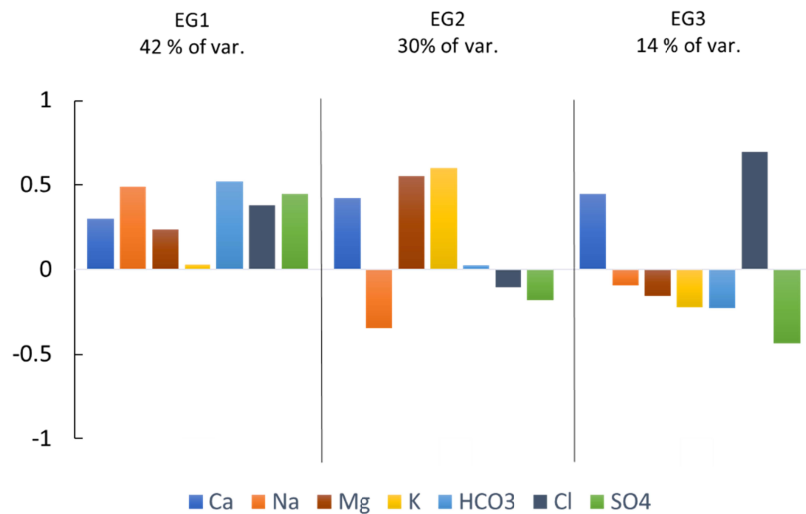
717 **Figure 11**. Contribution of eigenvectors 1, 2, and 3 to the total explained variance and relative contribution of each
718 species to each eigenvector.

719 The first eigenvector (EG1) explains 42% of the variance with similar positive contributions
720 from all solutes except K (0.03) (Figure 11). Solutes with a higher positive contribution are Na
721 (0.49), HCO_3 (0.52), SO_4 (0.45) and Cl (0.38). Therefore, EG1 seems to account for the main
722 chemical evolution of groundwater and is associated with evapoconcentration, silicate
723 weathering, calcite, and gypsum dissolution processes. Equal contribution in almost all solutes
724 suggests evapoconcentration is the most representative solute evolution process in EG1 (Figure
725 11).

726 The second eigenvector (EG2) explains 30% of the chemical variability and helps to distinguish
727 among processes responsible for dissolved cation (Ca, Na, Mg, and K) evolution in groundwater.
728 Two major processes identified based on EG2 contributions are biotite weathering (Section
729 3.1.1) responsible for increasing Ca, Mg and K concentrations (positive contribution in EG2,
730 Figure 11), and andesine weathering (Section 3.1.1) for increased dissolved Na (negative
731 contribution in EG2, Figure 11). Although calcite dissolution could also explain higher Ca
732 concentration in EG2, a higher contribution of HCO_3 would be expected.

733 The third eigenvector (EG3) explains 14% of the groundwater chemical variability, and Cl (0.69)
734 and Ca (0.44) are positively contributing to this EG while SO_4 contribution (-0.43) is negative
735 (Figure 11). We attribute the Cl increase to mixing between fresh water and seawater. The
736 positive Ca contribution in EG3 is related to the selection of the Ca-Cl end-member. This end-
737 member is the only sample of this groundwater type and by far has the highest dissolved Cl.
738 Negative SO_4 contribution is attributed to gypsum dissolution even though it is not followed by a
739 negative Ca contribution. We attribute this contradiction to the strong influence of the Ca-Cl
740 end-member. The positioning of non-seawater mixing samples (TLA01 and TLA02) with the
741 highest dissolved SO_4 and Na in Figure 12

742

743
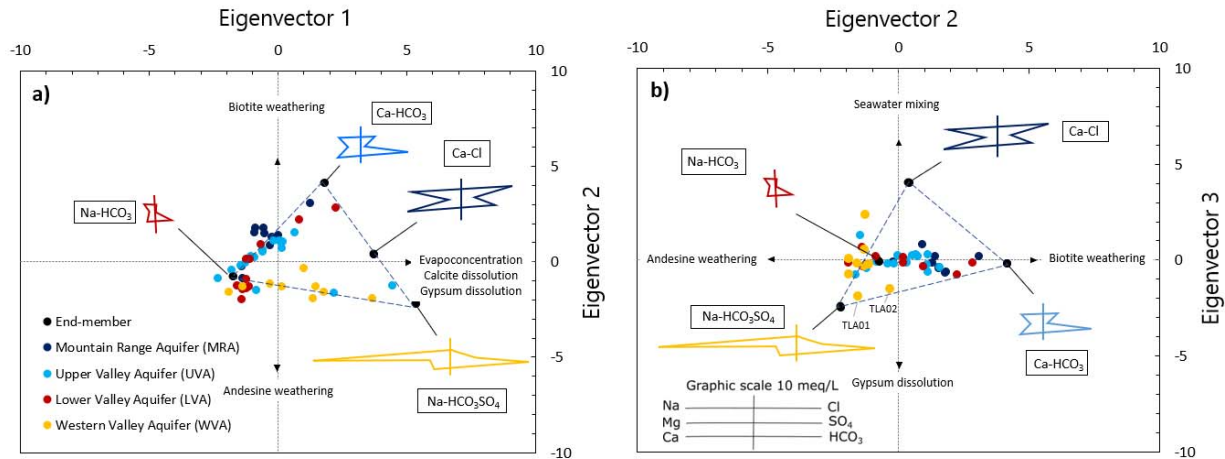
Figure 12a) Projection of solutes concentrations to the first and second eigenvectors space. B) Projection of solutes concentrations to the second and third eigenvectors space. Stiff diagrams represent the ion concentrations of selected end-members.

Based on these results, the main processes that drive Ca-HCO3 groundwater type (representative of MFR and shallow MBR) are biotite weathering, evapoconcentration, calcite dissolution and gypsum dissolution (Figure 12a and Figure 12b). Andesine and biotite weathering are the main processes influencing Na-HCO3 groundwater indicative of MBR (Figure Figure 12a and Figure 12b). The WVA groundwater is represented by the Na-HCO3SO4 groundwater type and is mainly affected by evapoconcentration, calcite dissolution, gypsum dissolution, andesine weathering, and sulfate reduction. Finally, the Ca-Cl groundwater type from this same region represents processes driven by evapoconcentration, calcite dissolution, gypsum dissolution and seawater mixing. These results agree with results obtained in Section 3.1.1 and confirm processes identified for each MSR process.

3.3.2. Improving EMMA by Considering Chemical Reactions

To further improve EMMA, main geochemical processes affecting each eigenvector are identified and chemical reactions are considered in four EMMA models (B, C, D, E and F Table 3). These models aim to reduce the non-conservative behavior of solutes and improve model performance. The model performance is evaluated using RMSE and R^2 instead of the total explained variance. The total explained variance is useful when comparing models with the same number of components. Chemical reactions are represented by conservative **u** components. Components and chemical reactions of each model are reported in Table 3.

765 **Table 3.** Chemical reactions along with the reacting species and conservative components of each model.

Chemical reactions	Components
A No chemical reactions	Na, Ca, Mg, K, Cl, SO_4 and alkalinity
B Andesine dissolution (Eq. 1)	$U_{Andesine} = Ca - 0.7Na$ Mg, K, Cl, SO_4 and alkalinity
C Andesine dissolution (Eq. 1) Biotite dissolution (Eq. 3)	$U_{Andesine} = Ca - 0.7Na$ $U_{Biotite} = Mg - 3K$ Cl, SO_4 and alkalinity
D Andesine dissolution (Eq. 1) Gypsum dissolution (Eq. 5)	$U_{And.-Gyp.} = Ca - 0.7Na - SO_4$ Mg, K, Cl and alkalinity
E Andesine dissolution (Eq. 1) Biotite dissolution (Eq. 3) Gypsum dissolution (Eq. 5)	$U_{And.-Gyp.} = Ca - 0.7Na - SO_4$ $U_{Biotite} = Mg - 3K$ Cl and alkalinity
F Andesine dissolution (Eq. 1) Biotite dissolution (Eq. 3) Gypsum dissolution (Eq. 5) Calcite dissolution (Eq. 8)	$U_{And.-Gyp.-Calc.} = Ca - 0.7Na - CO_3 - SO_4$ $U_{Biotite} = Mg - 3K$ Cl

766

767 Highly satisfactory results are obtained by incorporating chemical reactions into EMMA instead
768 of chemical solutes as indicated by improved R^2 and RMSE statistics (Table 2, Table 4, and
769 Figure S1). Model F has the best results with $R^2 = 0.9$, $0.1 \leq RMSE \leq 1.3$ and slopes between 0.8 to
770 1.1. As the number of components is equal to the number of end-members (three), 100% of the
771 variance is explained by the model. These results further validate all the proposed processes
772 driving the groundwater chemistry in Section 3.1.1. These results agree with Pelizardi et al.
773 (2017) where a synthetic model using simple solutes was compared to a synthetic model using
774 conservative components by computing two objective functions. Their results show that using
775 conservative components instead of simple solutes decreases the objective functions as species
776 affected by chemical reactions usually contribute to a higher percentage of the variance. A recent
777 study by Goyetche et al. (2022) applied the Pelizardi (2017) methodology to a coastal aquifer, by
778 using two conservative u components and one eigenvector. The first u component accounted for
779 four cation exchange and mineral dissolution reactions while the other u component accounted

780 for eight redox reactions. Their results showed that 97% of the variance could be explained by
781 the model.

782 **Table 5.** Results of EMMA analysis: coefficient of determination (R^2), root-mean-squared error (RMSE), and slope
783 (m), of major solutes, pH and stable $\delta^{18}O$, δ^2H, and $\delta^{13}C$ between measured and modeled concentrations for models
784 B to F.

Model	Variables																				
	Cl			Alk			SO$_4$			Mg			K			U-Andesine			U-Biotite		
	R^2	RMSE	m	R^2	RMSE	m	R^2	RMSE	m	R^2	RMSE	m	R^2	RMSE	m	R^2	RMSE	m	R^2	RMSE	m
B	0.8	0.9	0.6	0.6	2.0	0.5	0.7	0.4	0.7	0.8	0.2	0.7	0.5	0.04	0.4	0.8	1.3	0.7			
C	0.6	0.2	0.6	0.6	1.9	0.7	0.6	0.5	1.0							0.6	3.0	0.2	0.6	0.3	0.4
D	0.7	1.5	0.4	0.9	0.7	1.0				0.5	0.3	0.6	0.7	0.03	0.5	0.9	0.9	1.0			
E	0.9	0.7	1.2	0.6	2.0	0.5										0.9	1.1	0.9	0.8	0.2	0.7
F	0.9	0.7	1.1													0.9	1.3	0.8	0.9	0.1	0.9

785

3.4. Quantifying MBR and MFR Contributions to the Valley Aquifer System

787 The ratio of each MSR process to total recharge was computed by running MIX for model F
788 (Figure 13). One of the most important results is the high proportion of deep MBR recharging
789 the valley aquifer. Deep MBR represents more than 50% of the UVA and LVA groundwater
790 samples (the Na-HCO3 groundwater type). The high percentage of deep MBR in the UVA wells
791 supports the hypothesis of a mixing zone in the unconfined and confined aquifer contact (Figure
792 10). The MBR proportion increases up to 70% when the Na-HCO3SO4 groundwater type is also
793 considered. On average, MFR and shallow MBR accounts for 28% of recharge in the UVA, 17%
794 in the LVA, and 20% in the WVA regions. The MFR and shallow MBR contribution decreases
795 with increasing well depth and distance from the mountain front. These results are consistent
796 with the longer flow paths between the WVA wells and the Sierra Nevada. The WVA region has
797 a higher influence of seawater mixing as expected. Higher MBR contribution suggests greater
798 connectivity between the Sierra Nevada and the sedimentary basing groundwater. These results
799 agree with the recent studies highlighting the greater role of MBR compared to MFR (Markovich
800 et al., 2019; Meixner et al., 2016; Aishlin & McNamara, 2011; Manning and Solomon, 2003)
801 and can be used to better constrain future groundwater models for climate change assessment.
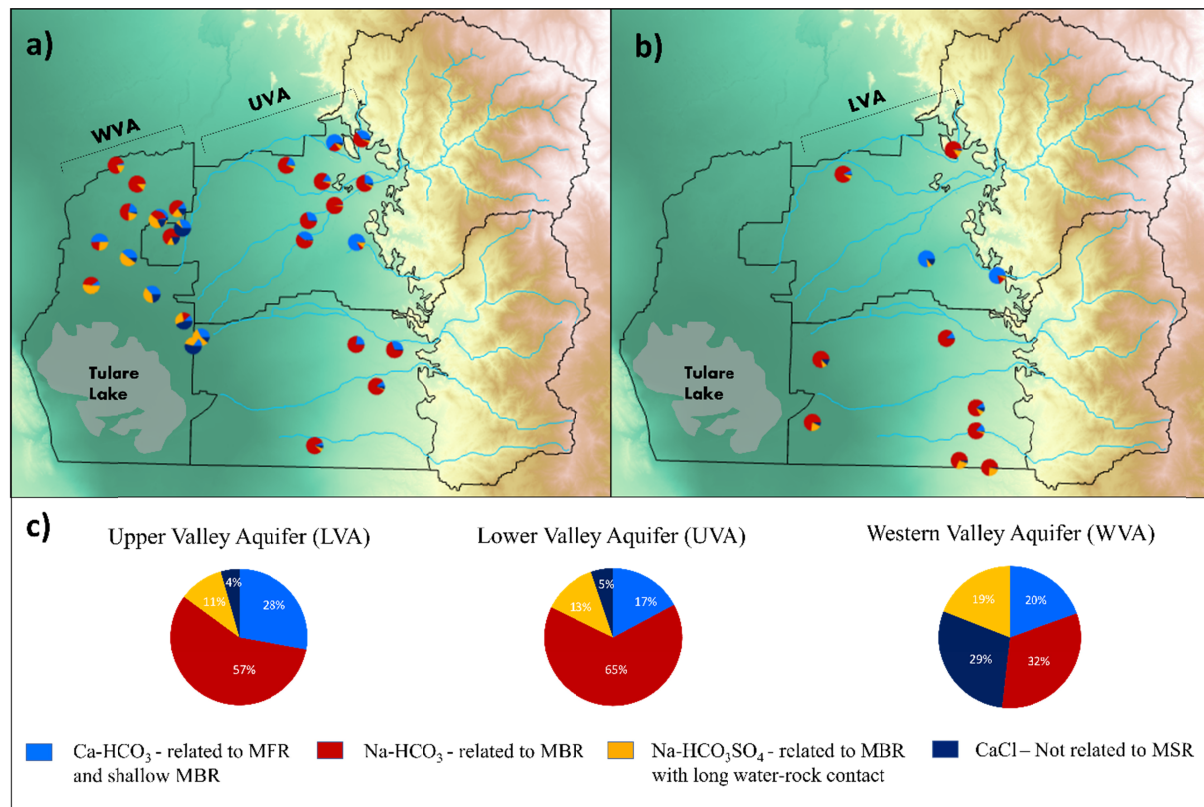
Figure 13. (a) Mixing ratios of each sample in the Upper Valley Aquifer (UVA) and Western Valley Aquifer (WVA) regions (b) and the Lower Valley Aquifer (LVA) region. (c) Average mixing ratios for each groundwater region.

4. Conclusions

We identified major hydrogeochemical processes responsible for the regional groundwater chemistry of the Sierra Nevada and northern Tulare basin to understand MSR pathways. These pathways include diffuse and focused MAR, MFR, and shallow and deep MBR. The main sources of MSR are rain and snowmelt that via direct infiltration through soil or surface water bodies influences mountain-valley groundwater chemistry. Groundwater isogeochemistry data distinguishes three recharge end-members in the valley groundwater that are influenced by hydrologic processes of mountain watersheds. MFR is associated with the evaporated $Ca-HCO_3$ groundwater type where its composition is influenced by evapoconcentration, edaphic CO_2 dissolution, biotite weathering, and calcite dissolution. Shallow MBR is mainly associated with the non-evaporated $Ca-HCO_3$ groundwater type and edaphic CO_2 dissolution, biotite weathering, and calcite dissolution affect its chemistry. The main source of shallow MBR is snowmelt infiltration during the peak snowmelt. MFR and shallow MBR recharge the first 100 m of the upper aquifer. Deep MBR is mainly associated with $Na-HCO_3$ and $Na-HCO_3SO_4$ groundwater type that are influenced by andesine weathering and gypsum dissolution and recharged during the peak of snowmelt. The MBR recharging the bottom of the confined aquifer is associated with evaporated $Na-HCO_3$ groundwater type where its chemistry is influenced by andesine weathering and focused MAR from lakes and mountain streams. This groundwater type has a residence time of more than 50 yr, and the influence of focused MAR chemistry highlights the importance of surface water bodies as recharge of deep valley groundwater.

826 EMMA and MIX analysis revealed the spatial distribution of each recharge process associated
827 with the major hydrogeochemical processes in groundwater. Considering four end-members in
828 EMMA produced satisfactory results explaining 86% of the chemical variance. These results
829 were further improved by considering water-rock reactions using conservative chemical
830 components, resulting in significant improvement in model performance. These results highlight
831 the importance of chemical reactions in EMMA and Mix analysis in cases where identifying
832 conservative solutes is challenging. Mixing ratios show that more than 50% of the groundwater
833 system is recharged by MBR originating from the Sierra Nevada. Higher percentage of MBR
834 contribution indicate greater connectivity between the Sierra Nevada and the valley aquifer than
835 previously thought (Meixner et al., 2016). These results have important implications for
836 groundwater resources availability under climate change due to projected changes in the Sierra
837 Nevada snowpack.

838 This study highlights the importance of jointly analyzing groundwater chemistry with isotopes
839 via a multi-tool approach to understand the main factors controlling groundwater systems and
840 identify the main recharge processes. To our knowledge, this is the first comprehensive
841 assessment of mountain block recharge processes in the Sierra Nevada demonstrating the role of
842 mountain aquifers and deep flow paths in recharging Central Valley. Similar studies in other
843 mountain ranges with similar bedrock and geological characteristics will improve understanding
844 of mountain system recharge processes, leading to sustainable groundwater management.

845 **Acknowledgments**

854 **Open Research**

855 Datasets for this research are available in Table S1 and Table S2 in Supporting Information. The

856 EMMA and MIX code is open source and available on https://h2ogeo.upc.edu/.

857

858

859

860

861 **References**

862 Aishlin, P., & McNamara, J. P. (2011), Bedrock infiltration and mountain block recharge
863 accounting using chloride mass balance. *Hydrological Processes, 25*(12), 1934-1948.
864 doi:10.1002/hyp.7950

866 Ajami, H., Troch, P. A., Maddock III, T., Meixner, T., & Eastoe, C. (2011). Quantifying
867 mountain block recharge by means of catchment-scale storage-discharge relationships. *Water*
868 *Resources Research*, *47*(4). doi:10.1029/2010WR009598

870 Alam, S., Gebremichael, M., Li, R., Dozier, J., & Lettenmaier, D. P. (2019). Climate change
871 impacts on groundwater storage in the Central Valley, California. *Climatic Change*, *157*(3), 387-
872 406. doi:10.1007/s10584-019-02585-5

874 Appelo, C. A. J., & Postma, D. (2005). *Geochemistry, groundwater and pollution*. CRC press.

876 Bales, R. C., Molotch, N. P., Painter, T. H., Dettinger, M. D., Rice, R., & Dozier, J. (2006).
877 Mountain hydrology of the western United States. *Water Resources Research*, *42*(8).
878 doi:10.1029/2005WR004387

880 Barnett, T. P., Adam, J. C., & Lettenmaier, D. P. (2005). Potential impacts of a warming climate
881 on water availability in snow-dominated regions. *Nature*, *438*(7066), 303-309.
882 doi:10.1038/nature04141

884 Barthold, F. K., Tyralla, C., Schneider, K., Vaché, K. B., Frede, H. G., & Breuer, L. (2011). How
885 many tracers do we need for end member mixing analysis (EMMA)? A sensitivity
886 analysis. *Water Resources Research*, *47*(8). doi:10.1029/2011WR010604

888 Bazuhair, A. S., & Wood, W. W. (1996). Chloride mass-balance method for estimating ground
889 water recharge in arid areas: examples from western Saudi Arabia. *Journal of Hydrology*, *186*(1-
890 4), 153-159. doi:10.1016/S0022-1694(96)03028-4

892 Bennett, G.L., V, Fram, M.S., Johnson, T.D., (2017), Groundwater-Quality Data in the Tulare
893 Shallow Aquifer Study Unit, (2014-2015): *Results from the California GAMA Priority Basin*
894 *Project: US Geological Survey data release*. doi:10.5066/F7BP00W8.

896 Berghuijs, W. R., Woods, R. A., & Hrachowitz, M. (2014). A precipitation shift from snow
897 towards rain leads to a decrease in streamflow. Nature climate change, 4(7), 583-586.
898 doi:10.1038/nclimate2246

900 Boiano, D. M., Weeks, D. P., Hemry, T. (2005), Sequoia and Kings Canyon National Parks,
901 California: water resources information and issues overview report. *Technical Report*
902 *NPS/NRWRD/NRTR 2005/333. National Park Service, Denver, Colorado, USA*.

903 Christophersen, N., & Hooper, R. P. (1992). Multivariate analysis of stream water chemical data:
904 The use of principal components analysis for the end-member mixing problem. *Water Resources*
905 *Research*, *28*(1), 99-107. doi:10.1029/91WR02518

Carrera, J., Vázquez-Suñé, E., Castillo, O., & Sánchez-Vila, X. (2004). A methodology to compute mixing ratios with uncertain end-members. *Water resources research*, *40*(12). doi:10.1029/2003WR002263

Clow, D. W., Mast, M. A., Campbell, D. H. (1996), Controls on surface water chemistry in the upper Merced River basin, Yosemite National Park, California. *Hydrological Processes, 10*(5), 727-746. doi:10.1002/(SICI)1099-1085(199605)10:5<727::AID-HYP316>3.0.CO;2-D

Clow D. W., Mast M. A., Bullen T. D., and Turk J. T. (1997) Strontium 87/strontium 86 as a tracer of mineral weathering reactions and calcium sources in an alpine/subalpine watershed, Loch Vale, Colorado. Water Resources Res. 33, 1335–1351.

Coes, A. L., Pool, D. R., Stonestrom, D. A., Constantz, J., Ferre, T., & Leake, S. A. (2007). Ephemeral-stream channel and basin-floor infiltration and recharge in the Sierra Vista subwatershed of the Upper San Pedro Basin, southeastern Arizona. *US Geol Surv Prof Pap*, 253-311.

Craig, H. (1961). Isotopic variations in meteoric waters. *Science*, *133*(3465), 1702-1703. doi:10.1126/science.133.3465.1702

Davis, G.H., Green, J. H., Olmsted, F. H., & Brown, D. W. (1959). Ground-water conditions and storage capacity in the San Joaquin Valley California (No 1469). *US Government Printing Office.*

De Vries, J. J., & Simmers, I. (2002). Groundwater recharge: an overview of processes and challenges. *Hydrogeology Journal*, *10*(1), 5-17. doi:10.1007/s10040-001-0171-7

Diepenbrock, A. (1933). Mount Poso oil field. *California Oil Fields*, *19*(2), 4-35.

Diffenbaugh, N. S., Swain, D. L., & Touma, D. (2015). Anthropogenic warming has increased drought risk in California. *Proceedings of the National Academy of Sciences*, *112*(13), 3931-3936. doi:10.1073/pnas.1422385112

Elnashar, A., Wang, L., Wu, B., Zhu, W., & Zeng, H. (2020). Synthesis of global actual evapotranspiration from 1982 to 2019. *Earth System Science Data Discussions*, *2020*, 1-42. doi:10.5194/essd-13-447-2021

Faunt, C. C., Sneed, M., Traum, J., & Brandt, J. T. (2016). Water availability and land subsidence in the Central Valley, California, USA. *Hydrogeology Journal*, *24*(3), 675-684. doi:10.1007/s10040-015-1339-x

Feth, J. H. F., Robertson, C. E., Polzer, W. L. (1964), Sources of mineral constituents in water from granitic rocks, Sierra Nevada, California and Nevada. *US Government Printing Office.*

Flint, A. L., Flint, L. E., Hevesi, J. A., & Blainey, J. B. (2004). *Fundamental concepts of recharge in the Desert Southwest: a regional modeling perspective* (Vol. 9, pp. 159-184). Washington, DC: American Geophysical Union.

952 Friedman, I. (1992), Stable isotope composition of waters in southeastern California 1. Modern
953 precipitation. *Journal of Geophysical Research: Atmospheres, 97,* 5795-5812.

954 Frink, J. W., & Kues, H. A. (1954). Corcoran Clay—A Pleistocene lacustrine deposit in San
955 Joaquin Valley, California. *AAPG Bulletin*, *38*(11), 2357-2371.
956

957 Frisbee, M. D., Phillips, F. M., Campbell, A. R., Liu, F., and Sanchez, S. A. (2011), Streamflow
958 generation in a large, alpine watershed in the southern Rocky Mountains of Colorado: Is
959 streamflow generation simply the aggregation of hillslope runoff responses?, Water Resour.
960 Res., 47, W06512, doi:10.1029/2010WR009391.
961

962 Frisbee, M. D., Tolley, D. G., & Wilson, J. L. (2017). Field estimates of groundwater circulation
963 depths in two mountainous watersheds in the western US and the effect of deep circulation on
964 solute concentrations in streamflow. *Water Resources Research*, *53*(4), 2693-2715.
965 doi:10.1002/2016WR019553
966

967 Fujii, R., Swain, W. C. (1995), Areal distribution of selected trace elements, salinity, and major
968 ions in shallow ground water, Tulare Basin, southern San Joaquin Valley, California. *US
969 Department of the Interior, US Geological Survey, 95*, 4048.
970

971 Garrels, R.M, & Mackenzie, F.T., (1967), Origin of the chemical composition of springs and
972 lakes, in Equilibrium concepts in natural water systems. *American Chemical Society, Advances
973 in Chemistry Series no. 67*, 222-242.doi: 10.1021/ba-1967-0067.ch010
974

975 Gleeson, T., & Manning, A. H. (2008). Regional groundwater flow in mountainous terrain:
976 Three-dimensional simulations of topographic and hydrogeologic controls. *Water Resources
977 Research*, *44*(10). doi:10.1029/2008WR006848
978

979 Goodrich, D. C., Williams, D. G., Unkrich, C. L., Hogan, J. F., Scott, R. L., Hultine, K. R., Pool,
980 D., Coes, A., & Miller, S. (2004). Comparison of methods to estimate ephemeral channel
981 recharge, Walnut Gulch, San Pedro River basin, Arizona. *Groundwater recharge in a desert
982 environment: the southwestern United States*, *9*, 77-99. doi:10.1029/009WSA06
983

984 Goyetche, T., Luquot, L., Carrera, J., Martínez-Pérez, L., & Folch, A. (2022). Identification and
985 quantification of chemical reactions in a coastal aquifer to assess submarine groundwater
986 discharge composition. *Science of the Total Environment*, *838*, 155978.
987 doi:10.1016/j.scitotenv.2022.155978
988

989 Hem, J. D. (1985). *Study and interpretation of the chemical characteristics of natural
990 water* (Vol. 2254). Department of the Interior, US Geological Survey.
991

992 Hilton, G.S., McClelland E.J., Klausing R. L., Kunkel F. (1963), Geology hydrology, and quality
993 of water in the Terra Bella-Lost Hills area, San Joaquin Valley, California. *USGS Open-File
994 Report*, 6347, 158.
995

Hooper, R. P. (2003). Diagnostic tools for mixing models of stream water chemistry. *Water Resources Research*, *39*(3). doi:10.1029/2002WR001528

Hooper, R. P., Christophersen, N., & Peters, N. E. (1990). Modelling streamwater chemistry as a mixture of soilwater end-members—An application to the Panola Mountain catchment, Georgia, USA. *Journal of Hydrology*, 116(1-4), 321-343. doi:10.1016/0022-1694(90)90131-G

Hoots, H. W., Bear, T. L., & Kleinpell, W. D. (1954). *Geological summary of the San Joaquin Valley, California*. California, Division of Mines.

Huber, N. K. (1987). *The geologic story of Yosemite National Park* (No. 1595). US Geological Survey.

Huth, A. K., Leydecker, A., Sickman, J. O., Bales, R. C. (2004), A two-component hydrograph separation for three high-elevation catchments in the Sierra Nevada, California. *Hydrological Processes, 18*(9), 1721-1733. doi:10.1002/hyp.1414

Inter-Agency Committee on Land Subsidence in the San Joaquin Valley. (1958). *Progress Report on Land-Subsidence Investigations in the San Joaquin Valley, California, Through 1957*. The Committee.

Kang, S., Knight, R., Goebel, M. (2022), Improved imaging of the large-scale structure of a groundwater system with airborne electromagnetic data. *Water Resources Research, 58*, e2021WR031439. doi:10.1029/2021WR031439

Kendall, C., & Coplen, T. B. (2001). Distribution of oxygen-18 and deuterium in river waters across the United States. Hydrological processes, 15(7), 1363-1393. doi:10.1002/hyp.217

Klausing, R. L., & Lohman, K. E. (1964). Upper Pliocene marine strata on the east side of the San Joaquin Valley, California. *US Geological Survey Professional Paper 475-D*, 14-17.

Lechler, A. R., & Niemi, N. A. (2012), The influence of snow sublimation on the isotopic composition of spring and surface waters in the southwestern United States: Implications for stable isotope–based paleoaltimetry and hydrologic studies. *Bulletin*, *124*(3-4), 318-334.

Liu, Y., & Yamanaka, T. (2012). Tracing groundwater recharge sources in a mountain–plain transitional area using stable isotopes and hydrochemistry. *Journal of Hydrology*, 464, 116-126. doi:0.1016/j.jhydrol.2012.06.053

Lofgren, B. E. & Klausing, R. L. (1969), Land subsidence due to groundwater withdrawal, Tulare-Wasco area, California. *US Government Printing Office*, 437.

Manning, A.H. & Solomon, D.K. (2003). Using noble gases to investigate mountain-front recharge. J. Hydrol. 275, 194–207.

Markovich, K. H., Manning, A. H., Condon, L. E., & McIntosh, J. C. (2019). Mountain-block recharge: A review of current understanding. *Water Resources Research*, *55*(11), 8278-8304. doi:10.1029/2019WR025676

Mast, M. A., Drever, J. I., & Baron, J. (1990). Chemical weathering in the Loch Vale watershed, Rocky Mountain National Park, Colorado. *Water Resources Research*, *26*(12), 2971-2978. doi:10.1029/WR026i012p02971

Maxey, G. B., & Eakin, T. E. (1949). Ground water in White River Valley, White Pine, Nye, and Lincoln Counties, Nevada.

Meade, R. H. (1967). *Petrology of sediments underlying areas of land subsidence in central California* (Vol. 497). US Government Printing Office.

Meixner, T., Manning, A. H., Stonestrom, D. A., Allen, D. M., Ajami, H., Blasch, K. W., Brookfield, A., Castro, C., Clark, J., Gochis, D., Flint, A., Neff, N., Rodell, M., Scanlon, B., Singha, K., & Walvoord, M. A. (2016). Implications of projected climate change for groundwater recharge in the western United States. *Journal of Hydrology*, *534*, 124-138. doi:10.1016/j.jhydrol.2015.12.027

Melack, J. M., Stoddard, J. L., Ochs, C. A. (1985), Major ion chemistry and sensitivity to acid precipitation of Sierra Nevada lakes. *Water Resources Research, 21*(1), 27-32. doi:10.1029/WR021i001p00027

Melack, J. M., Sadro, S., Sickman, J. O., & Dozier, J. (2020). *Lakes and watersheds in the Sierra Nevada of California: Responses to environmental change* (Vol. 5). Univ of California Press.

Molins, S., Carrera, J., Ayora, C., & Saaltink, M. W. (2004). A formulation for decoupling components in reactive transport problems. *Water Resources Research*, *40*(10). doi:10.1029/2003WR002970

Moran, J. E., Esser, B. K., Hillegonds, D., Holtz, M., Roberts, S. K., Singleton, M. J., & Visser, A. (2011). *California GAMA special study: Nitrate fate and transport in the Salinas Valley* (No. LLNL-TR-484186). Lawrence Livermore National Lab. (LLNL), Livermore, CA (United States). doi:10.2172/1122241

NADP. (2022). National Atmospheric Deposition Program, https://nadp.slh.wisc.edu/sites/ntn-ca75/

NOAA. (2022). National Water Model CONUS Retrospective Dataset was accessed on 2022 from https://registry.opendata.aws/nwm-archive.

Park, W. H., and Weddle, J. R. (1959), Correlation study of southern San Joaquin Valley. Summary of operations, *California oil fields, 45*(1), 33-34.

Parkhurst, D. L. (1997). Geochemical mole-balance modeling with uncertain data. *Water Resources Research*, *33*(8), 1957-1970. doi:10.1029/97WR01125

Pelizardi, F., Bea, S. A., Carrera, J., & Vives, L. (2017). Identifying geochemical processes using End Member Mixing Analysis to decouple chemical components for mixing ratio calculations. *Journal of Hydrology*, *550*, 144-156. doi:10.1016/j.jhydrol.2017.04.010

Peng, T. R., Zhan, W. J., Tong, L. T., Chen, C. T., Liu, T. S., & Lu, W. C. (2018). Assessing the recharge process and importance of montane water to adjacent tectonic valley-plain groundwater using a ternary end-member mixing analysis based on isotopic and chemical tracers. *Hydrogeology Journal*, *26*(6), 2041-2055. doi:10.1007/s10040-018-1741-2

Rose, T. P., Davisson, M. L., & Criss, R. E. (1996). Isotope hydrology of voluminous cold springs in fractured rock from an active volcanic region, northeastern California. *Journal of Hydrology*, *179*(1-4), 207-236. doi:10.1016/0022-1694(95)02832-3

Rosenthal, W., & Dozier, J. (1996). Automated mapping of montane snow cover at subpixel resolution from the Landsat Thematic Mapper. *Water Resources Research*, *32*(1), 115-130. doi:10.1029/95WR02718

Rueedi, J., Purtschert, R., Beyerle, U., Alberich, C., & Kipfer, R. (2005). Estimating groundwater mixing ratios and their uncertainties using a statistical multi parameter approach. *Journal of hydrology*, *305*(1-4), 1-14. doi:10.1016/j.jhydrol.2004.06.044

Scanlon, B.R., Reedy, R.C., Stonestrom, D.A., Prudic, D.E., Dennehy, K.F., (2005). Impact of land use and land cover change on groundwater recharge and quality in the southwestern US. Glob. Chang. Biol. 11, 1577–1593. https://doi.org/10.1111/j.1365-2486.2005.01026.x

Scanlon, B. R., Faunt, C. C., Longuevergne, L., Reedy, R. C., Alley, W. M., McGuire, V. L., & McMahon, P. B. (2012). Groundwater depletion and sustainability of irrigation in the US High Plains and Central Valley. *Proceedings of the national academy of sciences*, *109*(24), 9320-9325. doi:10.1073/pnas.1200311109

Schreiner-McGraw, A. P., Ajami, H., & Vivoni, E. R. (2019). Extreme weather events and transmission losses in arid streams. *Environmental Research Letters*, *14*(8), 084002. doi:10.1088/1748-9326/ab2949

Seager, R., Ting, M., Held, I., Kushnir, Y., Lu, J., Vecchi, G., Huang, H., Harnik, N., Leetmaa, A., Lau, N., Li, C., Velez, J., & Naik, N. (2007). Model projections of an imminent transition to a more arid climate in southwestern North America. *Science*, *316*(5828), 1181-1184. doi: 10.1126/science.1139601

Shaw, G. D., Conklin, M. H., Nimz, G. J., Liu, F. (2014), groundwater and surface water flow to the Merced River, Yosemite Valley, California: 36Cl and cl- evidence. *Water Resources Research, 50*(3), 1943–1959. doi:10.1002/2013WR014222

Sisson, T. W., & Moore, J. G. (1984). *Geology of Giant Forest-Lodgepole Area, Sequoia National Park, California*. US Department of the Interior, Geological Survey.

Tobin, B. W., & Schwartz, B. F. (2016). Using periodic hydrologic and geochemical sampling with limited continuous monitoring to characterize remote karst aquifers in the Kaweah River Basin, California, USA. *Hydrological Processes*, *30*(19), 3361-3372. doi:10.1002/hyp.10859

Visser, A., Moran, J. E., Hillegonds, D., Singleton, M. J., Kulongoski, J. T., Belitz, K., & Esser, B. K. (2016). Geostatistical analysis of tritium, groundwater age and other noble gas derived parameters in California. *Water Research*, 91, 314-330. doi:10.1016/j.watres.2016.01.004

Visser, A., Moran, J. E., Singleton, M. J., & Esser, B. K. (2018). Importance of river water recharge to the San Joaquin Valley groundwater system. *Hydrological Processes*, *32*(9), 1202-1213. doi:10.1002/hyp.11468

Viviroli, D., Kummu, M., Meybeck, M., Kallio, M., & Wada, Y. (2020). Increasing dependence of lowland populations on mountain water resources. *Nature Sustainability*, *3*(11), 917-928. doi:10.1038/s41893-020-0559-9

Wahi, A. K., Hogan, J. F., Ekwurzel, B., Baillie, M. N., & Eastoe, C. J. (2008). Geochemical quantification of semiarid mountain recharge. Groundwater, 46(3), 414-425. doi:10.1111/j.1745-6584.2007.00413.x

Wahrhaftig, C., & Birman, J. H. (1965). The Quaternary of the Pacific mountain system in California. In *The Quaternary of the US* (pp. 299-340). Princeton University Press.

Welch, L. A., & Allen, D. M. (2012). Consistency of groundwater flow patterns in mountainous topography: Implications for valley bottom water replenishment and for defining groundwater flow boundaries. *Water Resources Research*, *48*(5). doi:10.1029/2011WR010901

White, A. F., Bullen, T. D., Vivit, D. V., Schulz, M. S., & Clow, D. W. (1999). The role of disseminated calcite in the chemical weathering of granitoid rocks. Geochimica et Cosmochimica Acta, 63(13-14), 1939-1953. doi:10.1016/S0016-7037(99)00082-4

Williams, M., Kattelmann, R., & Melack, J. (1990). Groundwater contributions to the hydrochemistry of an alpine basin. *Hydrology in Mountainous Regions*, *1*, 741-748.

Williams M. W., Brown A. D., and Melack J. M. (1993) Geochemical and hydrologic controls on the composition of surface water in a high-elevation basin, Sierra Nevada, California. Limnol. Oceanogr. 38, 775–797.

Wilson, J. L., & Guan, H. (2004). Mountain-block hydrology and mountain-front recharge. *Groundwater recharge in a desert environment: The Southwestern United States*, *9*, 113-137. doi:10.1029/009WSA08

Xiao, M., Koppa, A., Mekonnen, Z., Pagán, B. R., Zhan, S., Cao, Q., ... & Lettenmaier, D. P. (2017). How much groundwater did California's Central Valley lose during the 2012–2016 drought?. *Geophysical Research Letters*, *44*(10), 4872-4879. doi:10.1002/2017GL073333

1177   Zhu, C., Winterle, J. R., & Love, E. I. (2003). Late Pleistocene and Holocene groundwater
1178   recharge from the chloride mass balance method and chlorine-36 data. *Water Resources*
1179   *Research*, *39*(7). doi:10.1029/2003WR001987